UNIVERSIDAD DE CHILE
FACULTAD DE CIENCIAS FÍSICAS Y MATEMÁTICAS
DEPARTAMENTO DE INGENIERÍA ELÉCTRICA

DEVELOPMENT OF AN INTEGRATED DOWN CONVERSION MODULE FOR W BAND

TESIS PARA OPTAR AL GRADO DE MAGÍSTER EN CIENCIAS DE LA INGENIERÍA, MENCIÓN ELÉCTRICA

ALEXANDER MARTIN IBARRA ESPINOZA

PROFESOR GUÍA:
NICOLÁS ANDRÉS REYES GUZMÁN

PROFESOR CO-GUÍA:
FAUSTO PATRICIO MENA MENA

MIEMBROS DE LA COMISIÓN:
MARCOS ANDRÉS DÍAS QUEZADA
FRANCISCO PIZARRO TORRES

Este trabajo ha sido parcialmente financiado por FONDECYT a través del proyecto Fondecyt 11151022, y el proyecto CASSACA.

SANTIAGO DE CHILE
2018

RESUMEN DE LA TESIS PARA OPTAR
AL GRADO DE MAGÍSTER EN CIENCIAS
DE LA INGENIERÍA, MENCIÓN ELÉCTRICA Y
AL TÍTULO DE INGENIERA CIVIL ELÉCTRICA
POR: ALEXANDER MARTIN IBARRA ESPINOZA
FECHA: 2018
PROF. GUÍA: SR. NICOLÁS ANDRÉS REYES GUZMÁN
PROF. CO-GUÍA: SR. FAUSTO PATRICIO MENA MENA

DEVELOPMENT OF AN INTEGRATED DOWN CONVERSION MODULE FOR W BAND

Atacama Large Millimeter Array (ALMA) es una asociación internacional entre Europa, América del Norte y el Este de Asia en cooperación con la República de Chile. Consiste en una arreglo de 66 antenas diseñadas para funcionar como un interferómetro. Cada antena tiene 10 receptores heterodinos sintonizados en diferentes bandas de frecuencia entre 30 y 950 GHz. El laboratorio de ondas milimétricas (MWL) de la Universidad de Chile está trabajando en un prototipo de receptor de la banda W Band extendida (Banda 2+3).

Esta tesis presenta el diseño, la construcción y la caracterización de un módulo [de conversión descendente] mejorado e integrado para el receptor. Este módulo implementa un separador de banda lateral (2SB), el cual unifica todas las componentes necesarias en un solo módulo, para obtener un receptor mas compacto.

El módulo consta de cuatros componentes. Un ecualizador basado en dos ramas con resistencias de película delgada integradas como el elemento básico para compensar la pendiente de ganancia, un filtro pasabanda acoplado con borde de microbanda, un amplificador de potencia basado en el circuito integrado de microondas monolítico (MMIC) HMC1144 y un Lange coupler encargado de separar la señal RF en 2 bandas laterales simultaneamente como es caracteristicos de los receptores 2SB.

RESUMEN DE LA TESIS PARA OPTAR
AL GRADO DE MAGÍSTER EN CIENCIAS
DE LA INGENIERÍA, MENCIÓN ELÉCTRICA Y
AL TÍTULO DE INGENIERA CIVIL ELÉCTRICA
POR: ALEXANDER MARTIN IBARRA ESPINOZA
FECHA: 2018
PROF. GUÍA: SR. NICOLÁS ANDRÉS REYES GUZMÁN
PROF. CO-GUÍA: SR. FAUSTO PATRICIO MENA MENA

DEVELOPMENT OF AN INTEGRATED DOWN CONVERSION MODULE FOR W BAND

The Atacama Large Millimeter Array (ALMA) is an international partnership between Europe, North America and East Asia in cooperation with the Republic of Chile. It consists of an array of 66 antennas designed to work as an interferometer. Each antenna has 10 heterodyne receivers tuned to different frequency bands between 30 and 950 GHz. The millimeter wave laboratory (MWL) of the University of Chile is working on a prototype W band extended receiver (Band 2 + 3).

This thesis presents the design, construction, and characterization of an upgraded and integrated [down-conversion] module for the lateral band separation receiver. This module implements a sideband separator (2SB), which unifies all the necessary components in a single module, to obtain a more compact receiver.

The module consists of four components. An Equalizer based on two branches with thin film resistances integrated as the basic element to compensate for the gain slope, a Microstrip Edge Coupled Bandpass Filter, a Power Amplifier based on the monolithic microwave integrated circuit (MMIC) HMC1144, and a Lange Coupler in charge of separating the RF signal in 2 lateral bands simultaneously as it is characteristic of the 2SB receivers.

Quiero agradecer a mi madre Jeanette, mis hermanos Paola e Ivan, también a mis amigos y Andrea por haberme apoyado en todo momento.

Tambien me gustaria agradecer a los profesores Nicolas Reyes y Patricio Mena quienes me orientaron y me entregaron los conocimientos necesarios. A Claudio Jarufe quien me guió durante el desarrollo de mi tesis. A mis compañeros de laboratorio de Ondas Milimétricas por su buena disposición y ayuda cuando la necesite.

A mis amigos del departamento de Eléctrica por todos los buenos momentos y enseñanzas.

Contents

Chapter 1

INTRODUCTION

1.1 Context

Karl Jansky was a scientist who worked in Bell's Laboratories studying the properties of the ionosphere as a source of interference to the transatlantic radiotelephony service. Using short waves, he concluded that the radiation received could not come from the Sun, but that it came from outside our Solar System, and that it was stronger in the direction of the center of the galaxy. It was in 1933 when his study was published in the New York Times [0]. Subsequently, in 1965 the radiation of cosmic background was measured accidentally by Arno Penzias and Robert Woodrow Wilson when they were using a Dicke radiometer for experiments of satellite communications. The discovery of the cosmic back radiation was very important since it corroborates the Big Bang theory and the demonstration that the universe is expanding. This two experiments allowed the advancement of observations in the range of the non-visible spectrum [0].

The electromagnetic (EM) spectrum can be classified according to its wavelength or frequency. These characteristics are related by $c = \lambda \times f$ (1.0), where λ , c, and f are the wavelength, the speed of light, and the frequency respectively. The EM spectrum is classified in different ranges depending on its frequency. The range that includes waves with wavelengths between 10 and 0.1 [mm] is known as millimetric and submillimetric regime. The associated frequencies go from few gigahertz to some terahertz. In astronomy, this frequency range is used to observe and study the cold universe, dust clouds, and star formation zones [0]. However, to obtain observations in this frequency range, exceptional atmospheric conditions are necessary, since the atmospheric absorption is particularly high in millimeter wavelengths.

The north area of Chile exhibits low levels of pollution light, low levels of electromagnetic radiation, and high altitude (5000 meters above sea level). To add on, the dryness of the Atacama Desert achieves a very low amount of water vapor and exhibits approximately 300 cleared days a year [0]. This makes Chile an ideal place for astronomical observations. It is for this reason that a large number of observatories have chosen this privileged location for it is operations. Among these, it is possible to highlight ALMA (Atacama Large Millimeter / Submillimeter Array) observatory, located on the Chajnantor plain. This telescope has an

observation capability from the 30 at 950 [GHz] divided into 10 frequency bands as seen in table 1.1 [0][0].

Table 1.1: Alma frequency bands.

Band Number	Frequency Range [GHz]	Wavelength [mm]
1	31.3-45	6.7-9.6
2	67-90	3.3-4.5
3	84-117	2.6-3.6
4	125-163	1.8-2.4
5	163-211	1.4-1.8
6	211-275	1.1-1.4
7	275-374	0.8-1.1
8	385-500	0.6-0.8
9	602-720	0.4-0.5
10	787-950	0.3-0.4

The receiver of band 2 works from 67 to 90 [GHz] and the receiver of band 3 works from 84 to 117 [GHz], existing an important overlap between them. So there is a possibility of unifying the receivers of band 2 and 3 into one receiver covering the entire bandwidth 67 to 117 [GHz]. It is intended that this new receiver occupies only the space allocated to one receiver. If that is the case, the freed space could be used as the location of a new receiver for a new observation band.

Figure 1.1 shows the top view of the cryostat, with the distribution of the different frequency bands

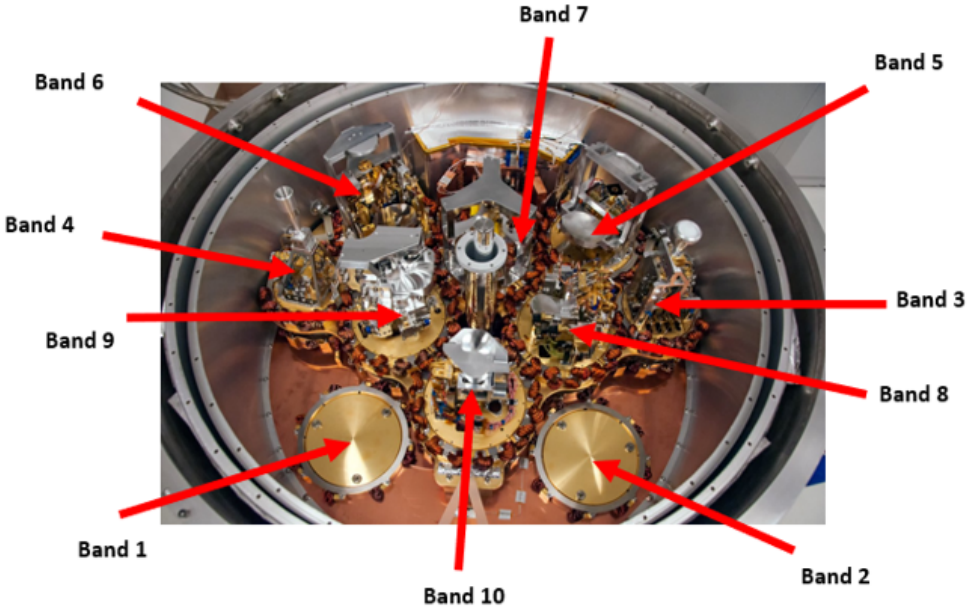

Figure 1.1: Top view of the cryostat, with the distribution of the different bands [0].

One of the new interests of ALMA is to produce a single receiver that could cover the entire frequency range of 67 to 117 [GHz], covering Band 2 and Band 3 in a single receiver

cartridge, a system called Band $2+3$. That is why the Departments of Electrical Engineering and Astronomy of the University of Chile are working together for a Band $2+3$ receiver in the Millimetric Wave Laboratory of the National Astronomical Observatory in Cerro Calan [0].

The objective of this thesis is to present the design and manufacture of fundamental components for the new receiver of the Band $2+3$. We focus our work mainly on the design a power amplifier, an equalizer, a Lange coupler, and a bandpass filter. These components will then be assembled in a compact 2SB reception module for the W band.

Currently, the construction of receivers is a challenge and solutions have varied from modular designs to integrated designs. Generally, each component of the receiver is manufactured in a separate block, but this increases the size of the final receiver. Therefore, it is desirable to have the ability to assemble the components in the minimum amount of blocks, thus, in turn, reducing the final size. The new receiver is also associated with the possibility of being able to increase the number of elements to observe, building a multiple beam receiver [0]-[0]. The possibility of obtaining a multiple beam image would allow observing extended astronomical sources faster than conventional single-beam while maintaining a comparable level of performance [0].

1.2 Hypothesis

• The new receiver will be capable of achieving an operational bandwidth equivalent to the bands $2 + 3$.

• The Power Amplifier will deliver a power over 15 [dBm] between 40 to 60 [GHz], delivering upper power than necessary 6 [dBm] for the operation of the sub harmonic mixer.

• The Equalizer will be able to compensate the 5 [dB] gain slope produced inside the Band $2 + 3$ by the RF amplification stage.

• The Filter will allow to select signals inside the band $2 + 3$ with low return losses -10 [dB] and reject signals outside the Band with a slope of losses per insertion greater than -2 [dB/GHz].

• The Lange coupler will allow a sideband rejection greater than 20 [dB] inside the Band $2 + 3$, which satisfies the minimum requirements.

1.3 General Objectives

The objective of this work is to design a module for the sideband separation receiver (2SB) in the range of millimeter waves (specically W band).

1.4 Specific Objectives

The specific objectives of this Thesis project are the following:

• Design a Power Amplifier based on the MMIC HMC1144, which operates between 40 to 60 [GHz]. The design must comply with the electrical and mechanical requirements for its manufacture.

• Built the required Power Amplifier.

• Carry out the necessary tests to compare the measurements obtained with the expected results.

• Design an Edge Coupled Microstrip Bandpass Filters for the $2 + 3$ band from 67 to 117 [GHz].

• Design an Equalizer for the $2 + 3$ band from 67 to 117 [GHz] with gain slope greater than 5 [dB].

• Design a Lange Coupler for the $2 + 3$ band from 67 to 117 [GHz].

1.5 Thesis Structure

In chapter 2 the necessary concepts are given to understand the components that any receiver has, and what is its function. Concepts are also delivered to understand the techniques used in the design and interpretation of results.

Chapter 3 presents the design of the amplifier and the results obtained from the simulations, as well as fabrication and subsequent assembly to obtain the final amplifier. Some tests made to the amplifier are also presented in order to obtain their behavior and the results are compared with the expected values.

Chapter 4 details the steps to follow to design an Edge Coupled Microstrip Bandpass Filters to Band $2 + 3$, the simulations and its final design.

Chapter 5 details the steps to follow to design an Equalizer with 5 [dB] of gain to Band $2+3$, the simulations and its final design.

Chapter 6 details the steps to follow to design a Lange Coupler to Band $2+3$, the simulations, and its final design.

Finally, in chapter 7, final conclusions and recommendations are presented for each of the components.

Chapter 2

GENERAL CONCEPTS

In this section, we present the different types of receivers, with their operating diagrams and the limitations in their components. We also present here the architecture of the prototype conversion module, which is the fundamental objective of this work. It will also be necessary to introduce a few concepts related to the development of components.

2.1 Mixer Theory

One of the main elements in any receiver is the mixer. It allows the process of heterodination, which consists in converting the received RF signal into a lower frequency signal. The majority of mixer types combine the RF input signal with the LO (Local Oscillator), delivering the sum and difference of the two frequencies at the output [0][0]:

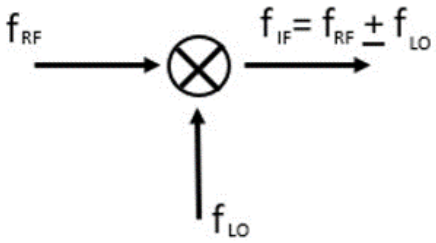

Figure 2.1: Fundamental mixer block diagram.

In some cases, it is necessary to use more than one mixer, as in the typical 2SB receivers, so it is necessary that these require low power and occupy the least possible space.

2.1.1 Schottky diode

The Schottky diode is one of the most used microwave mixers. The non-linearity of a Schottky diode is what ultimately allows it to be used as a mixer. Its design consists of a pair of metal contacts mounted on opposite ends of a doped semiconductor. It is possible to use type N and P diodes, although N-type GaAs are preferably used than silicon due to the properties of higher carrier velocity. Which translate into higher operation frequency. To this is added the fact that it is the material with the highest barrier potential in the metal-semiconductor interface.

The non-linearity of the device can be seen represented by equation 2.1, where I represent the saturation current of the diode, e is the charge of the electron, V is the voltage applied across the terminals of the diode, is a factor that denotes the efficiency of the diode which generally varies between 1 and 10, k is the Boltzmann constant and T is the temperature of the diode.

$$I = I_{sat} * \left(\mathrm{e}^{qV/nKT} - 1\right) \tag{2.1}$$

The cutoff or maximum frequency of the diode is determined mainly by parasite effects of capacitance and resistance of the materials that constitute it and is given by:

$$f_c = \frac{1}{2\pi R_s C_j} \tag{2.2}$$

Where R_s and C_j represents the shunt resistance and the barrier capacitance, formed by the parasitic accumulation of charges in the semiconductor when there is no voltage present [0][0].

2.1.2 Sub-harmonic mixer

The Sub-harmonic mixers can achieve the same cut off frequency as fundamental mixers, but they require an LO the signal with a fraction of the frequency required in a fundamental mixer.

The advantages of this configuration are that they are more immune to the DC voltage offset at their output, and to the second order intermodulation frequency (IM) than the fundamental mixers. However, conversion losses are greater[0].

The Schottky diode, it is generally used to produce a Sub-harmonic mixer, where the LO frequency is multiplied internally, producing a mixture of RF frequency components and an integer multiple of LO frequency, as shown in figure 2.2:

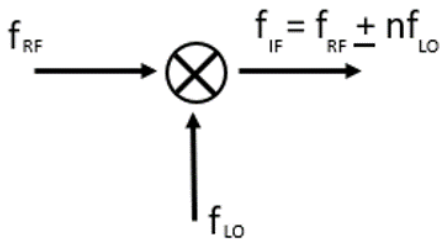

Figure 2.2: Subharmonic mixer block diagram.

If F_{RF} , *and* F_{Lo} are the radio frequency input signal and the input signal of the oscillator then it will have n frequency output signals, where n is the order of the subharmonic mixer [0][0].

2.2 Types of Receivers

In general, the task of every RF receiver consists of converting a received signal to a fixed intermediate frequency (IF) which can be more conveniently processed than the original carrier frequency. As a result of this conversion normally results in two mirror-image sidebands. The signal components above the carrier frequency constitute the upper sideband (USB), and those below the carrier frequency constitute the lower sideband (LSB).

Receivers are classified mainly by the different ways of separating the desired signal from the image signal, and the components used. Below are the typical configurations used:

2.2.1 Double Sideband Configuration (DSB)

The DSB configuration is the simplest one to be used, and also occupies the least number of components. In figure 2.3 a, a typical DSB configuration is presented. Because the signals picked up by the antenna are weak, in the order of few μW, a LNA (Low Noise Amplifier) is required. The amplified RF signal is combined with the (LO) signal and directed to the mixer, which converts the RF signal into an Intermediate Frequency (IF) signal so that it can be digitized later. This IF signal is a representation of the RF signal but at a lower frequency. Subsequently, the IF signal passes through a bandpass filter to eliminate the harmonics produced by the mixing process. Finally, it is necessary to carry out a new amplification of the IF signals. The final signal from the DSB receiver corresponds to the superposition of the (LSB) and the (USB), which increases the noise in the converted signal downwards and, therefore, in the observation time [0][0]

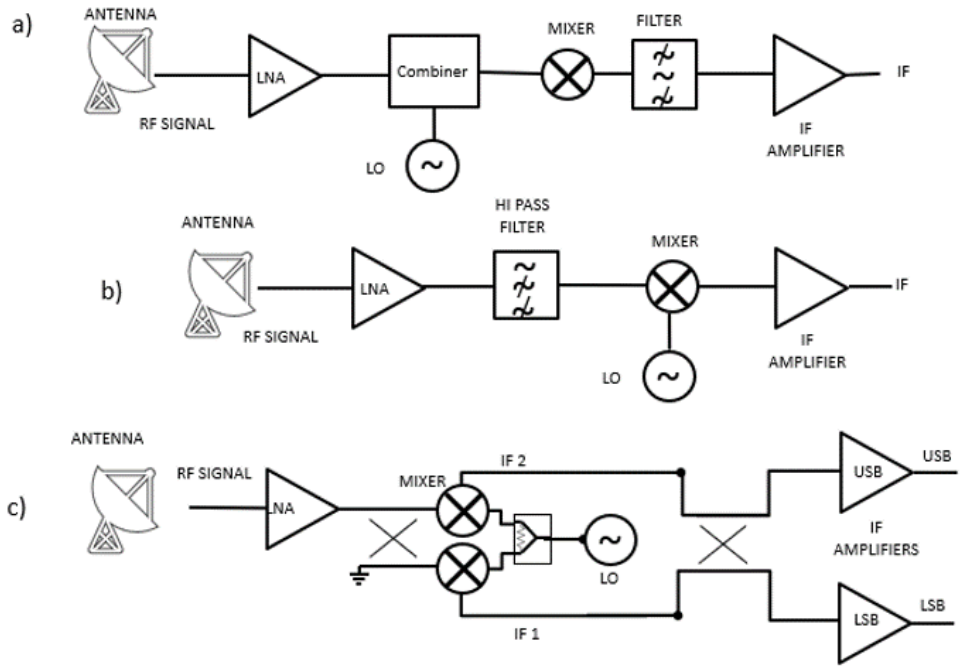

Figure 2.3: a) Schematic of a DSB heterodyne receiver. b) Schematic of an SSB receiver. c) Schematic of a 2SB receiver.

2.2.2 Single Sideband Configuration (SSB)

The single sideband (SSB) configuration differs from the DSB because a filter is added before the mixer. This filter has the purpose of eliminating one of the bands resulting from the downward conversion. In figure 2.3 b shows, as an example of a high pass filter. This filter avoids the problem of spectrum overlap, but at the cost of losing half of the RF Bandwidth [0][0].

2.2.3 Configuration of sideband separation (2SB)

The 2SB configuration solves the problems of the previously mentioned configurations because it allows observing the two lateral bands simultaneously independently. This reduces the noise in each sideband by a factor of two and increases the bandwidth of the observations, but with a complexity in the receiver architecture. In this configuration, the use of a hybrid or a Lange coupler becomes fundamental as it allows separating the RF signal in two signals with the required 90° a phase shift between the outputs. This configuration has the disadvantage that the rejection of the lateral band depends on the amplitude and the phase imbalance of the entire system [0]-[0].

2.3 Proposed design

The fundamental objective of this work is the design and construction of compact modules of down conversion in the band from 67 to 117 [GHz]. Figure 2.4 presents a diagram of the receiver module being developed.

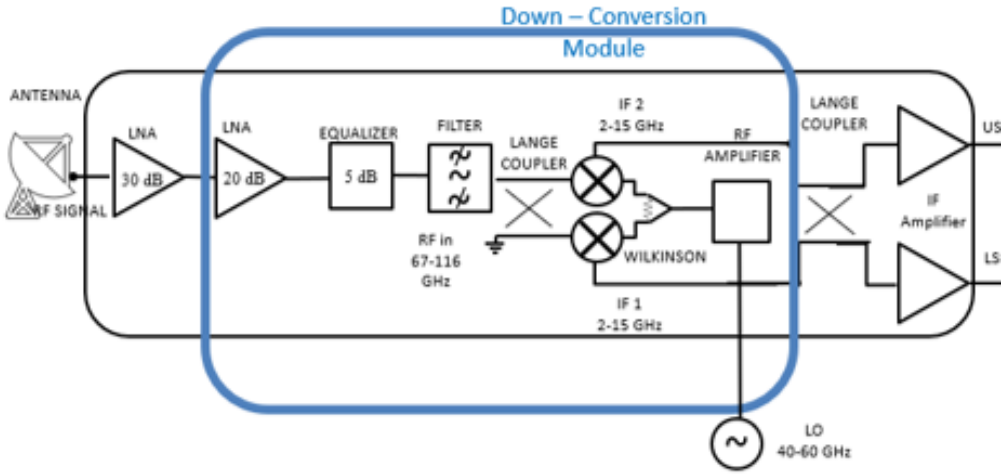

Figure 2.4: Schematic of Module Down Conversion based a DSB heterodyne receiver. The module consists of a series of components, a LNA low noise amplifier to compensate for weak signals received, an equalizer which compensates for the attenuation produced in the initial amplification stage, a filter in charge of allowing transmission of signals in the W band, and reject others And a lange coupler in charge of separating the RF signal, adding a 90° phase shift between the outputs

2.3.1 Low Noise Amplifier (LNA)

Due to the fact that the noise of a receiver is determined by its first component, it is necessary to use a LNA in the first place [0][0]. For the design of the proposed down conversion module. We chose the MMIC (microwave monolithic integrated circuit) CGY2190UH from OMMIC [0], which operates in the W band with an exceptionally low noise figure of 2.8 [dB] at 90 [GHz] combined with an ultra low power of 30 [mW].

These amplifiers were assembled and tested in our laboratory at room temperature and cryogenic operation [0]. The results of the characterization of the amplifiers showed a gain greater than 19 [dB] and a noise temperature less than 100 [K] when operating at 20 [K]. However, the amplifier had a gain roll-off at a high frequency.

For the design of the receiver proposed in this thesis, it is necessary to use two cascaded MMICs to achieve adequate gain for the amplification stage.

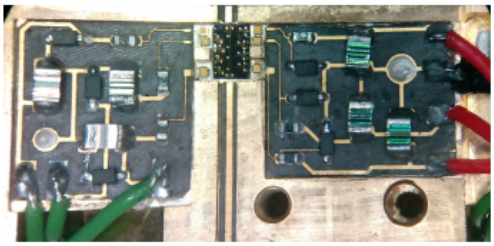

Figure 2.5: Picture of the amplifier CGY2190 from OMMIC. The chip is shown packaged with microstrip input and output in a test block. Credits: Claudio Jarufe.

2.3.2 Equalizer

The equalizer is used as a second element to compensate the attenuation of 5 [dB] in the upper part of the W band produced in the initial amplification stage. The design will consist of a circuit with two resonant RLCs in cascade to obtain the necessary 5 [dB]. These resonators will be designed based on microstrip lines and surface mount resistors. In chapter 4 more details on the design of this component will be presented.

2.3.3 Filter

A bandpass filter will be used to allow transmission in the band $2 + 3$ and reject the others. There are numerous ways to design filters in microstrip, but coupled transmission lines are one of the most commonly used due to its easiness of design, low cost and that it can be designed with small dimensions. More details about the microstrip filter design can be seen in chapter 5.

2.3.4 Lange Coupler

As mentioned before, the Lange coupler allows you to separate the RF signal into two identical signals by reducing its power by -3 [dB] and adding a 90° phase shift between the outputs. Then, the IF1 and IF2 signals are recombined in another Lange coupler producing the cancellation of the lateral bands, allowing it to obtain the USB and LSB separated. This Lange coupler will be designed based on microstrip lines. Chapter 6 will present more details about the design of this coupler.

2.3.5 Mixer

The mixers available in the market are packed in large blocks, so, in the Laboratory of Millimeter Waves of the University of Chile, it was decided to build sub-harmonic mixers based on Schottky diodes using MMIC technology.

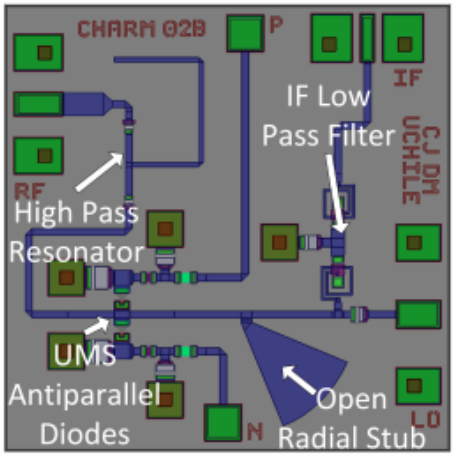

Figure 2.6: Layout of the subharmonic mixer for the extended W-band design [0]. The total die size is 1×1 $[mm^2]$. The pads designated with P and N are for positive and negative bias respectively.

In figure 2.6 it is possible to observe a layout of Subharmonic mixer designed with MMIC technology to operate in the W band [0], in which the frequency selected for IF ranges from 2 to 15 [GHz]. Two mixers were designed, the first requires a power of 13 [dBm] for LO at the lower frequencies, and above 104 [GHz] more power is needed. Conversion losses are better at 13 [dB] across the band. In the other design, it was based on a biased subharmonic mixer, which allows to decrease the power for the LO to 0 [dBm], with conversion losses better than 20 [dB] in almost the entire band [0].

2.3.6 Power Amplifier

Unlike the LNA, a (PA) is a circuit for converting DC input power into a significant amount of RF microwave output power. The PA usually takes signals with a high SNR (signal to noise ratio) from the circuits and increases its power. A wide variety of active transistors are currently available for use in RF power amplifiers. They are based on indium phosphide, silicon, gallium arsenide, among others. Table 2.1 shows the physical characteristics of some semiconductor materials [0].

It is possible to see in table 2.1 that the electron mobility in GaAs and InP is higher than in Si, which increases the transistor frequency beyond 300 [GHz] microwave region. Moreover, the higher drift velocities of electrons in SiC and GaN boosts the current gain of the device, resulting in high output power.

Table 2.1: Valor parameters final design to the final block.

Characteristic	Si	GaAs	InP	GaN
Electron mobility $u_n[cm^2/Vs]$	1500	8500	5400	1250
Thermal conductivity $\lambda[W/cm.K]$	1.5	0.46	0.68	1.3
Electron drift velocity $V_{sat}[x10^7 cm/s]$	1	1	1	2.2

The smaller thermal conductivity of GaAs and InP compared with Si causes increased substrate heating. It is for this reason that these devices are suitable for operation at low power

levels. In comparison, the higher thermal conductivity of SiC results in better heat dissipation and device reliability. GaN and Si can produce five times more power compared with GaAs and InP based PAs because of its high thermal conductivity and high break down voltage.

Silicon CMOS technology is very popular in industries because of its low cost, low supply voltage, and high integration capability. However, its low breakdown voltage, low operation speed and increased leakage due to scaling are serious drawbacks at millimeter wave frequencies. For higher power requirements such as airborne radar, ship radar, and military applications, GaN-HEMT is the best candidate at lower frequencies while InP-HBT is well suited for high frequencies above 300 [GHz] [0][0][0].

A HEMT transistor is a special type of MOSFET transistor, in which a joint made of a semiconductor material such as GaAs is made, and a compound that includes a metal, usually AlGaAs. The presence of this junction causes a barrier of potential along with it. As a consequence, the electrons that are located along the joint are forced or trapped in there. Unlike traditional HEMTs, mHEMTs place an intermediate layer of aluminum-indium arsenide (AlInAs). The advantage of this construction is that it is easy to obtain any concentration of Indium in the channel, allowing the transistor to be optimized according to its application [0][0][0].

In this thesis, we use the commercial MMIC HMC1144, which is a pHEMT (pseudomorphic High Electron Mobility Transfer) of gallium arsenide (GaAs) because it provides 19 [dB] (typical) of gain in the operating band 35 to 70 [GHz]. The MMIC has its inputs and outputs internally matched to 50 [ohms]. For its implementation, it is necessary to design an adaptation block, which will be described in chapter 3 [0].

2.4 Scattering Parameters

In microwave engineering the preferred representation of the behavior of a linear network is the $S-$parameters. When working at high frequencies, the $S-$parameters allow to describe any $N-$ ports networks by relating the incident voltage waves in the ports v^-, with those reflected from the ports v^+[0][0].

$$\begin{bmatrix} V_1^- \\ V_2^- \\ \vdots \\ \vdots \\ V_N^- \end{bmatrix} = \begin{bmatrix} S_{11}S_{12}\cdots & S_{1N} \\ S_{21}S_{22}\cdots & S_{2N} \\ S_{21}S_{22}\ddots & S_{3N} \\ \vdots & \vdots \\ S_{N1}S_{N2}\cdots & S_{MN} \end{bmatrix} \begin{bmatrix} V_1^+ \\ V_2^+ \\ \vdots \\ \vdots \\ V_N^+ \end{bmatrix} \tag{2.3}$$

2.5 Noise

The signals that reads the receiver are so weak that they are easily confused with the noise produced by electronic components. These noises can be due to different factors, but one of the main ones is the thermal noise, which is the product of the natural movement of particles in a material that is at a temperature different from absolute zero. In radiocommunications, to express the noise generated by a certain equipment, the concept of equivalent temperature of noise is used. This represents the power generated by a device that is to be characterized by [0]:

$$P_r = KT_{eq}B \tag{2.4}$$

Where K, T_{eq} , and B represent the boltzmann constant, the equivalent noise temperature of the system, and the bandwidth of the signal.

An important concept is that when we have more than one component connected, it is possible to find the equivalent temperature of the complete set by means of the well-known "Friis formula" [0]:

$$T_{\mathrm{eq}} = T_1 + \frac{T_2}{G_1} + \frac{T_3}{G_1 * G_1} + \cdots \tag{2.5}$$

Where G_{i} is the gain of each component i.

The Friis formula allows the generalization of the results to two or more stages in cascade, where the noise temperature of the first material of the sequence will be preponderant. It is for this reason that the first element in the receiver is a low noise amplifier.

Another quantity that it also used in the description of components is the figure of noise, which is given by the logarithmic relation between the equivalent temperature of equipment noise, and T_0 which is a reference temperature [0][0][0].

$$NF = 10\log_{10}(1 + \frac{T_{eq}}{T_0}) \tag{2.6}$$

2.6 Summary

In this chapter we reviewed the most important concepts for this thesis. Starting with a brief introduction to the operation of the mixers, a description of the configurations of the receivers, a description of the proposed receiver, and its components. Also introduced concepts necessary for the development of work, such as noise and parameters S.

Chapter 3

POWER AMPLIFIER

As mentioned in chapter 2, a power amplifier is a circuit for converting DC input power into a significant amount of RF microwave output power. This power RF is required by the mixer to carry out the down-conversion process. The construction of a power amplifier with a high gain also allows the possibility of generating a focal plane array. The potential of a multi-beam imaging system is of great interest in radio astronomy because it would allow observing extended astronomical sources faster than traditional single beam or phased array telescopes, maintaining a comparable level of performance.

The design of the amplifier was made in the range of 40 to 60 [GHz], this because the design was based on a subharmonic mixer, so the LO requires operating in the middle of the RF band 80 to 120 [GHz].

The design of the power amplifier is based on a monolithic integrated microwave circuit (MMIC) HMC1144, based on (GaAs). This MMIC operates from 40 to 70 [GHz] providing 19 [dB] of gain. The inputs and outputs are internally adapted to 50 [Ω], it is for this reason that the design of the adaptation block is necessary to channel the output signal of the rectangular waveguide of dimensions $4.775\ x\ 2.388\ [mm^2]$(known as standard WR19), to the amplifier by a microstrip line with impedance of 50 [Ω], as it is observed in the diagram of figure 3.1[0].

In this chapter, the design of the adaptation block is described, consisting of an adaptation from waveguide rectangular to microstrip. The adaptation block should work between $40-60$ [GHz].

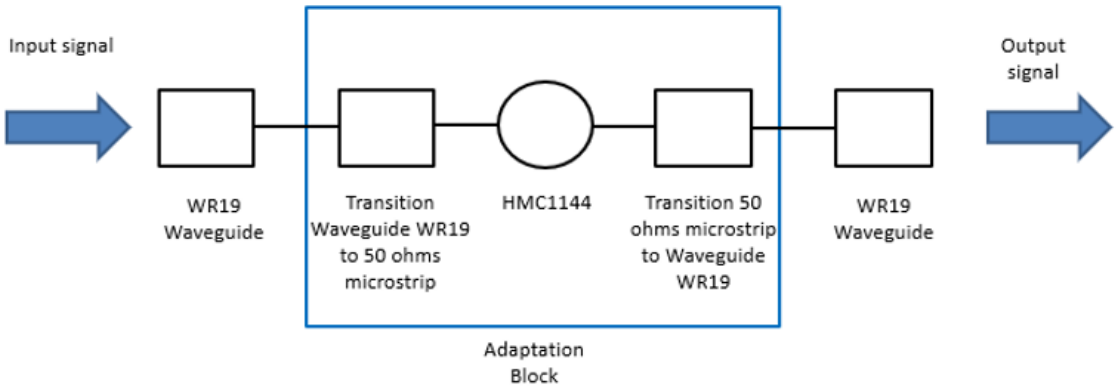

Figure 3.1: Adaptation block diagram. It is possible to observe that the input signal comes from a rectangular waveguide. This signal goes through a transition from rectangular waveguide to microstrip, in order to amplify it. Subsequently, the output signal of the amplifier must pass through a microstrip transition to a rectangular waveguide [0].

The commercial device HMC1144 was used for the design of the amplifier. This is a monolithic microwave integrated circuit (MMIC) of (GaAs) fabricated by Analog Devices [0]. This power amplifier will operate from 40 to 70 [GHz] providing 19 [dB] (typically) of gain, a P_{sat} of 20 [dB] over the entire bandwidth.

[a] 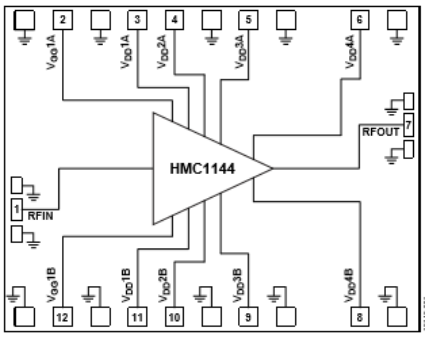

[b] 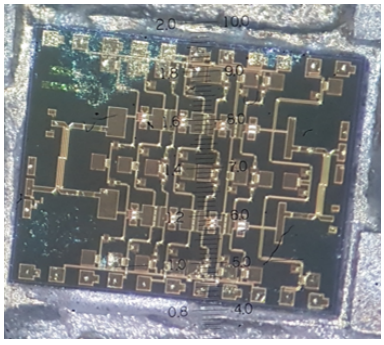

Figure 3.2: a) Functional block diagram. b) Photo of the HMC1144.

Figure 3.2 shows a diagram of the pads and a picture of the amplifier connections. The amplifier uses a balanced configuration with 4 stages of amplification, which allows minimizing possible interference, in the amplification stage. The RF inputs and outputs are made using a 50 [Ω] microstrip.

The MMIC must be polarized for its operation with a drain voltage of 4[V] and a current of 320 [mA], typically. It also needs a gate voltage between -2 to 0 [V] to control the current in the circuit, and therefore the total device gain [0].

3.1 Transition Waveguide-Microstrip line

The microstrip line is frequently used because it is relatively easy to manufacture. It has small dimensions, an easy integration into microwave circuits, and low cost [0]. A rectangular waveguide to microstrip transition was designed to route the signal coming to the amplifier over the entire bandwidth with the lowest possible reflections. Therefore, the design will be restricted so that the reflection coefficient is lower than -20 [dB] from 40 to 60 [GHz] [0][0]. The dimensions of the microstrip are 1.5×1 [mm^2], with a lower cut-off frequency of 100 [GHz], well above our target range, 40-60 [GHz] [0].

The dimensions of the rectangular waveguide are those determined by the band WR19 (39.2-59.6 [GHz]), which are 4.775×2.388 [mm^2] [0]. For the design of the adaptation antenna, the dimensions of the rectangular cavity are chosen to avoid the propagation of the fundamental TE10 rectangular waveguide mode.

Previous work [0]-[0] have proposed waveguide probe transitions with RF bandwidths of less than 35 percent. The design proposed here is based on the design of a radial which provides a better performance in term of bandwidth, compared with rectangular pieces [0].

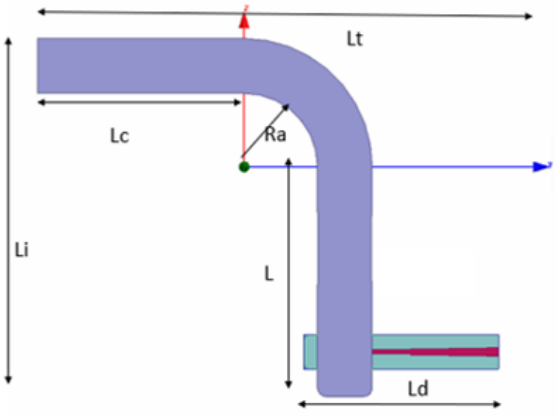

Figure 3.3: Schematic of transition from rectangular waveguide to microstrip.

The transition design was performed in the software HFSS, from ANSYS, as shown in figure 3.3. A well known microwave substrate was chosen for the microstrip of line, Duroid 5880, which is characterized by its relative constant of 2.2 and its thickness of 0.127[mm].

For the mechanical design, it was considered that the minimal sensitivity to mill the inside of the rectangular waveguide is 1 [mm] in diameter. Using this measurement were curved the backshort and the capacitive waveguide step, as shown in figure 3.4. This modification adds a capacitive effect improving the results obtained in the simulations.

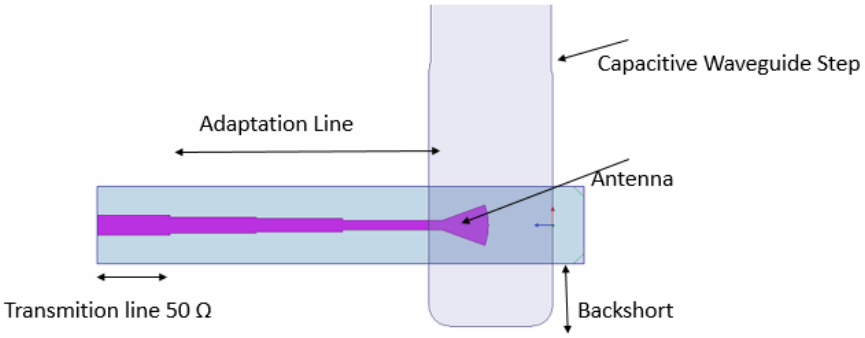

Figure 3.4: Schematic of the Antenna design.

The final result of the optimization of the design parameters are presented in table 3.1. The figure 3.5 show reflections lower than -20 [dB] in almost all the bandwidth, except around 55 [GHz] where they are less than -19 [dB]. These results satisfy the design requirements of the transition.

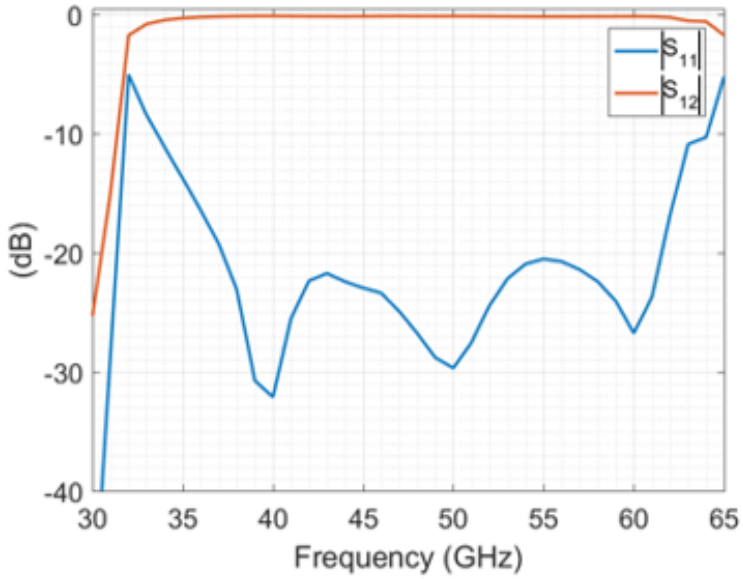

Figure 3.5: Result of the final simulation in HFSS. The red curve represents the transmission coefficient and the blue curve represents the reflection coefficient.

Table 3.1: Final design of parameter values.

Parameter	mm
L	10
R_a	3.2
L_c	9
L_{d}	9.6
L_t	21
L_{i}	21.5

3.2 Construction of transition block

Once the transition block was designed with the specified requirements (low reflections), the mechanical design was done using SolidWorks.

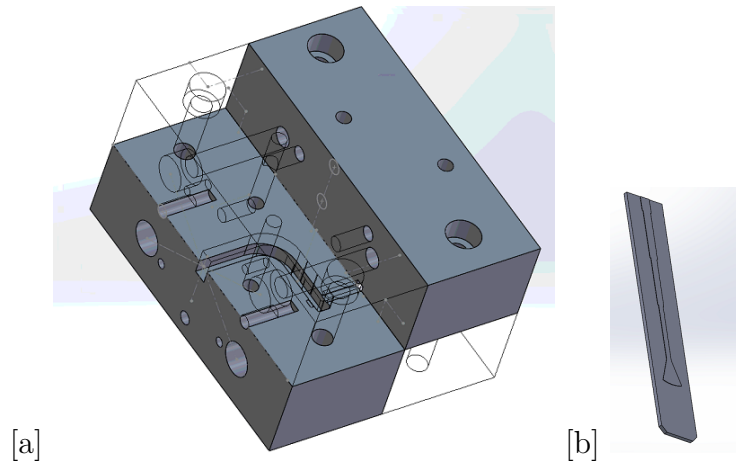

[a] [b]

Figure 3.6: a) Block design of adaptation in Solidworks. b) Design of the antenna.

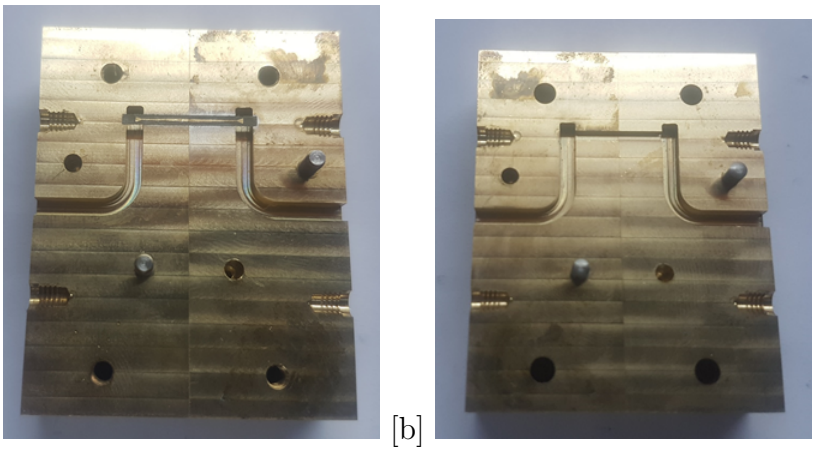

[a] [b]

Figure 3.7: a): a) Photo of the lower adaptation block, the block size is 52 × 21 × 15 $[mm^3]$. b) Photo of the top Adaptation block, the block size is 52 × 21 × 15 $[mm^3]$.

Subsequently, the microstrip antennas were fabricated using a laser LPKF printer, and after they were mounted on the block. For this last point, it was necessary to be very meticulous, because it is necessary to precisely glue the antenna to the block achieving the required alignment between components. Once the antennas were mounted, it was necessary to make the connection between both blocks to measure the losses in the transmission back to back. For this, the bonding machine model 4526 of the company Kulicke & Soffa was used. This machine allows making the electrical connection between the blocks as it is observed in figure 3.8.

[a] 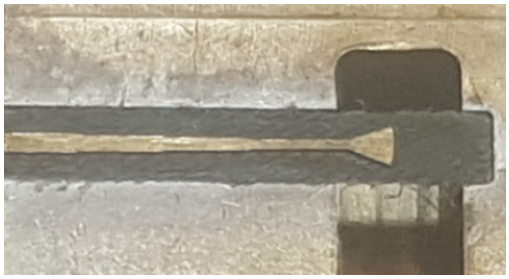 [b] 

Figure 3.8: a) Forum mounting antenna in adaptation block. b) Photo of bonding between adjustment blocks for back to back measurement.

3.3 Transmission of the measurement back to back

After assembling the antenna in the adaptation block and making the electrical connection between them, experimental measurements of the transmission coefficient were made. We used the signal generator (CXA Signal Analyzer) with an adapter module that allows to work up to 50 [GHz]. As a detector, the spectrum analyzer (PXA Signal Analyzer) was equipped with an harmonic mixer. The complete system was controlled by a LabVIEW Interface.

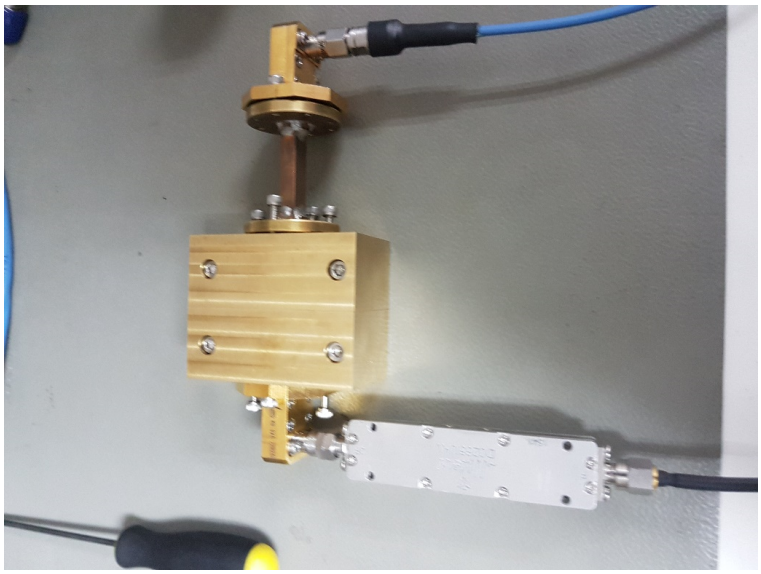

Figure 3.9: Connection photo of the CXA and PXA with the adaptation block, the block size is $52 \times 21 \times 30$ $[mm^3]$.

Once connected the CXA and the PXA with the adaptation block, measurements of transmission back to back in the adaptation block were made. These measurements allows to estimate the losses in the transitions to continue with the complete assembly. Results are presented in figure 3.10, the red curve represents the simulation performed in HFSS, and the blue curve the measurements obtained. It was noticed that on average, between 35 to 50 [GHz] there is approximately 2.2 [dB] of loss in the transmission, which is acceptable. At the

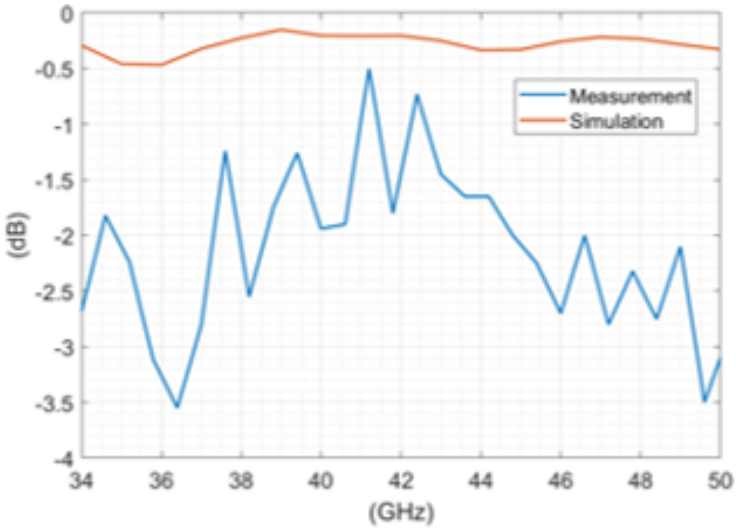

Figure 3.10: Result of the transmission measurement and the HFSS simulation. The red curve represents the transmission simulated and the blue curve the transmission measured.

time of the measurements of transmission back to back, there was no transition that allowed to measure frequencies higher than 50 [GHz]. The differences between the simulated and obtained results can be attributed to different factors that generate losses in the transition, such as the correct alignment and assembly of the antenna. Another important factor is the losses in the waveguide.

3.4 Design and Construction block HMC1144

After measuring the back-to-back transition and verifying that it works within the established margins, we proceeded to design and construct the block for the amplifier and the protection circuits.

3.4.1 Polarization HMC1144

Figure 3.11 shows the design scheme of the HMC1144. The dimensions of the integrated circuit are $2.3 \times 1.8 \times 0.05$ [mm^3] . According to the datasheet it is recommended to use 100 pF decoupling capacitors and 0.1 [μF] protection capacitors for the internal circuit. Since it is needed to power the amplifier with two voltages, V_{d} (Drain Voltage) and V_g (Gate voltage), it was necessary to fabricate two protection circuits.

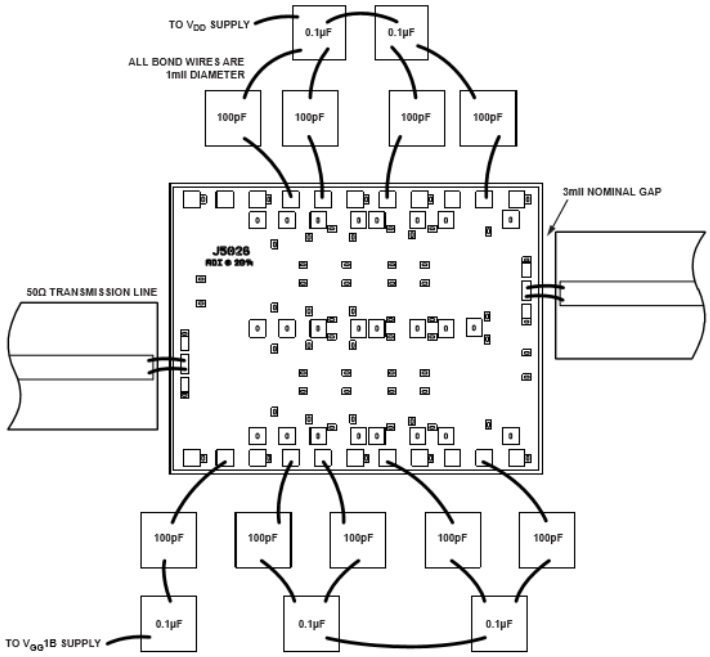

Figure 3.11: Connections Diagram, taken from datasheet [0].

[a] 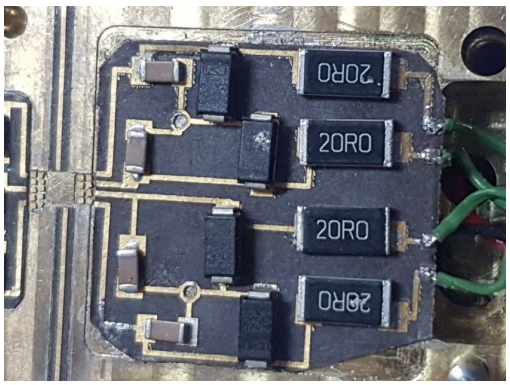 [b] 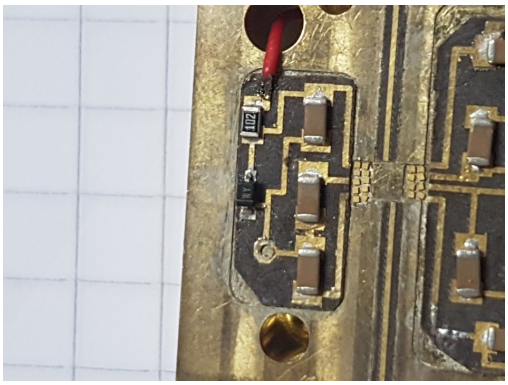

Figure 3.12: a) Photo of protection circuit 4 [V]. b) Photo of protection circuit -2 [V].

According to the datasheet, the value of V_{d} must be 4 [V], for which 4 protection circuits were manufactured based on Zener diode that allows to protect the MMIC. The value of Vg must be between -2 [V] and 0 V, which allows regulating the Drain current between 320 to 350 [mA]. Therefore, a protection circuit was manufactured with a maximum voltage of -2 [V].

3.4.2 Manufacture of support block for the HMC1144

Once the protection circuits were designed and manufactured, we proceeded to design the block for the MMIC and the microstrip lines necessary for the connection. At the time of designing the block, caution was exercised in aligning the inputs and outputs of the amplifier, as shown in figure 3.11. It was also necessary to place alignment pins and bolts for the subsequent assembly.

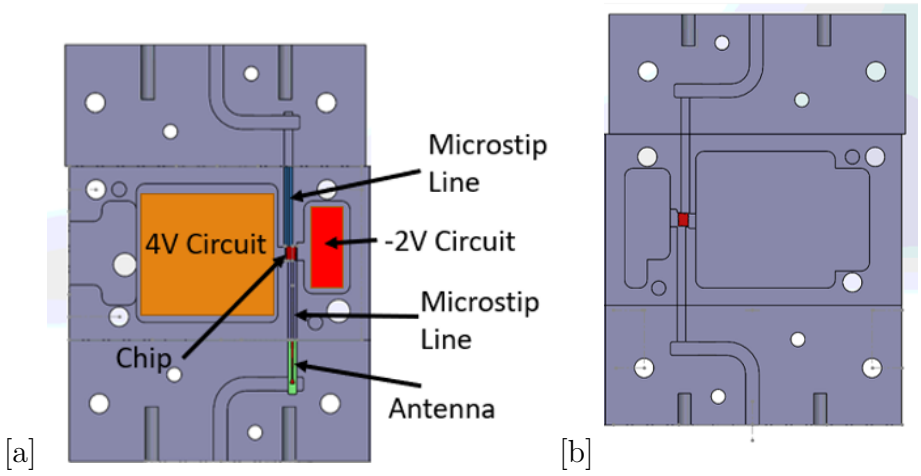

Figure 3.13: Block design for the MMIC. a) Lower block, the block size is $52 \times 72 \times 15$ $[mm^3]$.B) Upper block, , the block size is $52 \times 72 \times 15$ $[mm^3]$.

One the block was fabricated, first, the polarization circuits were mounted using silver paint to achieve electrical contact between the ground line of the manufactured PCB and the block. It was necessary a careful application of the silver paint, to avoid a short between the block and the feeding line.

Then, we proceeded to mount the antennas and decoupling capacitors (C1206) with great caution because the latter are small, so they are difficult to manipulate.

Once the protection circuits were assembled, the connector of the block was assembled and cables were welded to the protection circuits. Finally, the MMIC chip was added, taking care about its centered.

After, assembling all the components it was necessary to make the electrical connection between them using the bonding machine. Unfortunately, figure 3.14 shows that the bonding output is longer than recommended (3 to 6 [mil]), which can generate losses due to inductive effects.

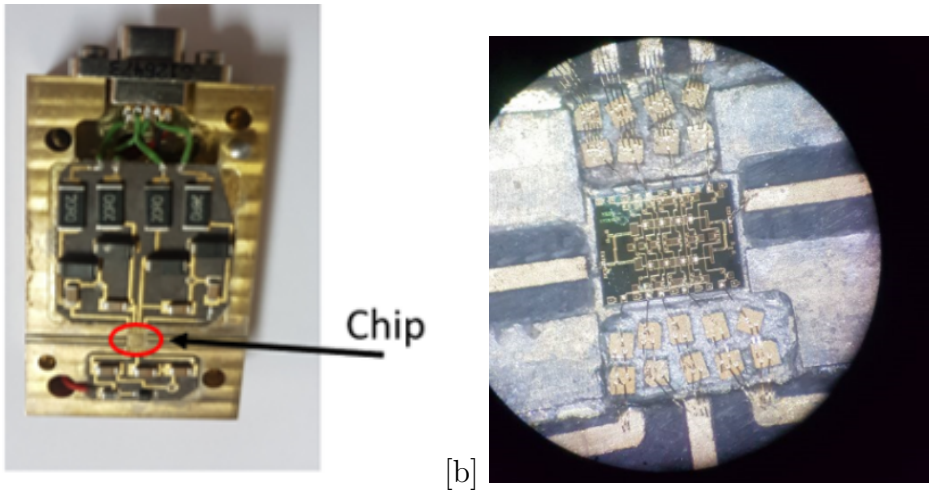

[a] [b]

Figure 3.14: a) Photo of assembly chip. The block size is 52 ×30×15[mm^3]. b) Photo of bonding chip and decoupling capacitors.

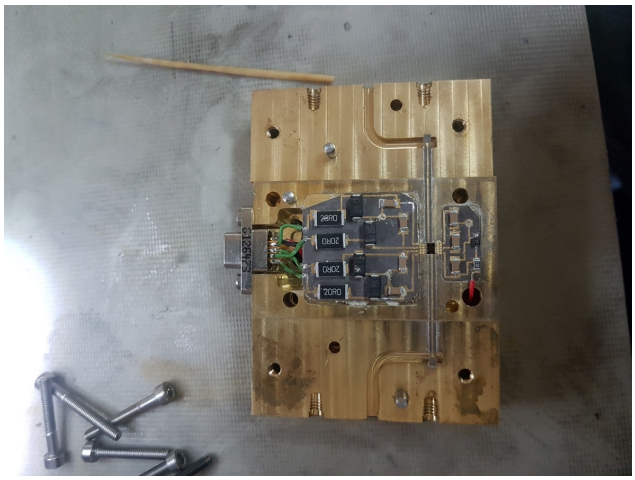

Figure 3.15: Photo of the final block with all the components, the block size is 52 × 72 × 15 [mm^3].

3.4.3 Measurements

Once the support block for the HMC1144 was built, the waveguide transition blocks were electrically connected to the microstrip by means of bondings, and the complete block was characterized using the VNA.

The VNA has to be initially calibrated to discount the effect of the cables and connectors on the measurements.

After calibration, the input and output ports were connected to the amplifier and the polarization connector to a high precision DC source (Keithley model 2612A). The bias point was 2,5 [V] of drain and gate voltage was controlled between 0 and −2 [V] to obtain the desired drain current between 320 to 350 [mA]. Figure 3.16 shows a photo of amplifier connected to the VNA and the external connector for bias.

Figure 3.16: Photo of connection of VNA with final block.

In figure 3.17 it is possible to observe the parameters S measured with the VNA, for a drain voltage of 2,5 [V], a drain current 320 [mA] and a Gate current $-0,001$ [mA].

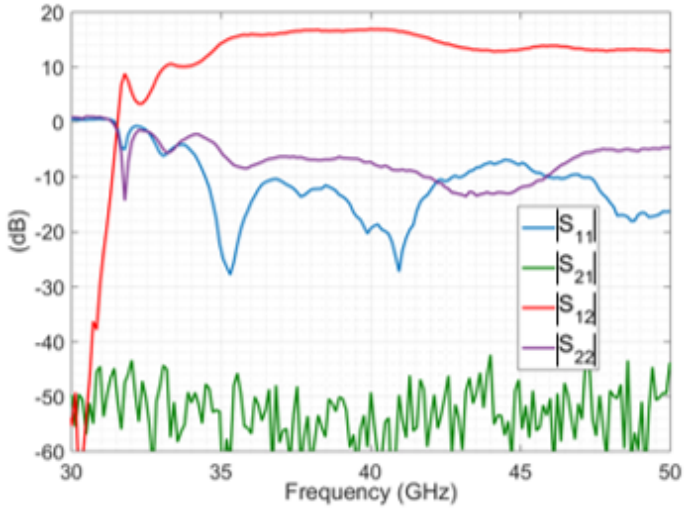

Figure 3.17: S parameters measured with the VNA, for a voltage 2,5 [V] drain, one drain 320 [mA] current and one gate -0.001 [mA] current.

The package amplifier setting with the parameters indicated above, shows a gain over 15 [dB] between 35 to 41 [GHz] $|S_{21}|$ and at higher frequencies, its gain drops significantly to approximately 13 [dB] between 43 to 50 [GHz]. The reflection of the input signal $|S_{11}|$ is less than -10 [dB] between 35 to 42 [GHz] and about 47 [GHz], but in the rest of the band increases about -8 [dB]. The reflection of the output signal $|S_{22}|$ is approximately less than -10 [dB] between 35 to 47 [GHz] and increases considerably as the frequency over 47 [GHz] increases. The isolation $|S_{12}|$ is practically zero, its value is less than -40 [dB].

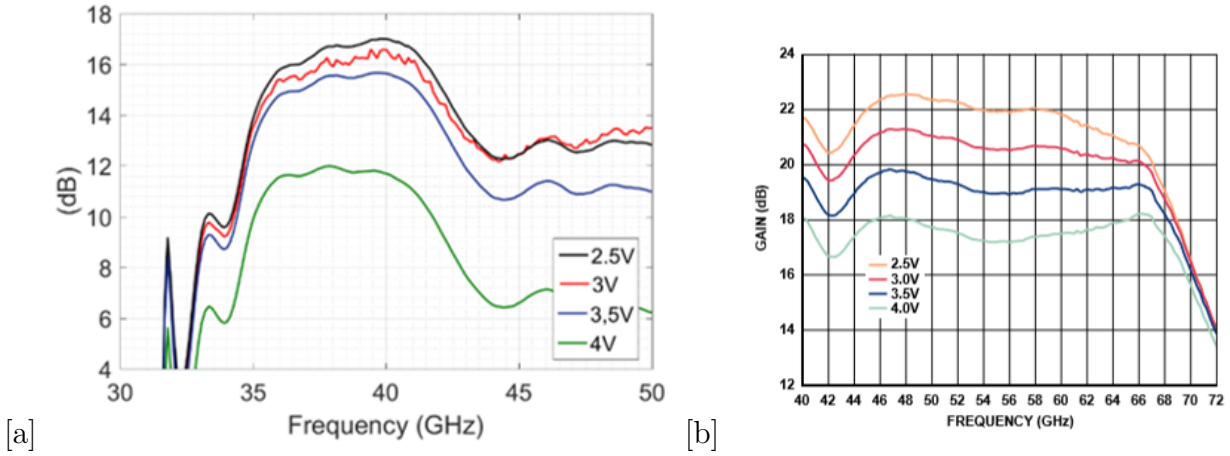

Figure 3.18: a) Experimental gain vs. frequency at various drain voltages. b) Theoretical gain vs. frequency at various drain voltages.

In figure 3.18 the experimental measurements of the gain obtained for different drain voltages are compared with the curves of the MMIC datasheet [0]. Due to limitations of our electronic equipment, it was only possible to characterize the MMIC up to 50 [GHz]. It is possible to observe that the curves measured experimentally differed from the manufacturer's data even in more than 5 [dB] around some frequencies. It is important to highlight that the gain delivered by the manufacturer corresponds to measurements made directly in the terminals. In contrast, our experimental measurements correspond to the fully packaged amplifier and some factors could unwanted losses.

An important factor is that the mounting the antenna may not have been totally straight, and differences of a few [μm] can cause unwanted changes in the results. For this reason, the transmission loss of the waveguide to microstrip adaptation blocks was previously measured, obtaining an average of 2.2 [dB] of loss in all the bandwidth.

Another important factor is the manufacture of the bondings. Although the bondings are necessary to make the electrical connections, it is recommended that they are as small as possible to avoid losses due to inductive effects. The length of the output bonding of the amplifier is considerably longer than the recommended one, to observe what effect introduces this in our results was simulated the bonding effects in AWR. The figures in 3.19 show the results obtained in AWR, where it is possible observer that the bonding length generates a loss in the gain of approximately 1.5 [dB] around the desired band.

These two factors mentioned above, give us an indication of why the performance of our amplifier is not like that delivered by the manufacturer.

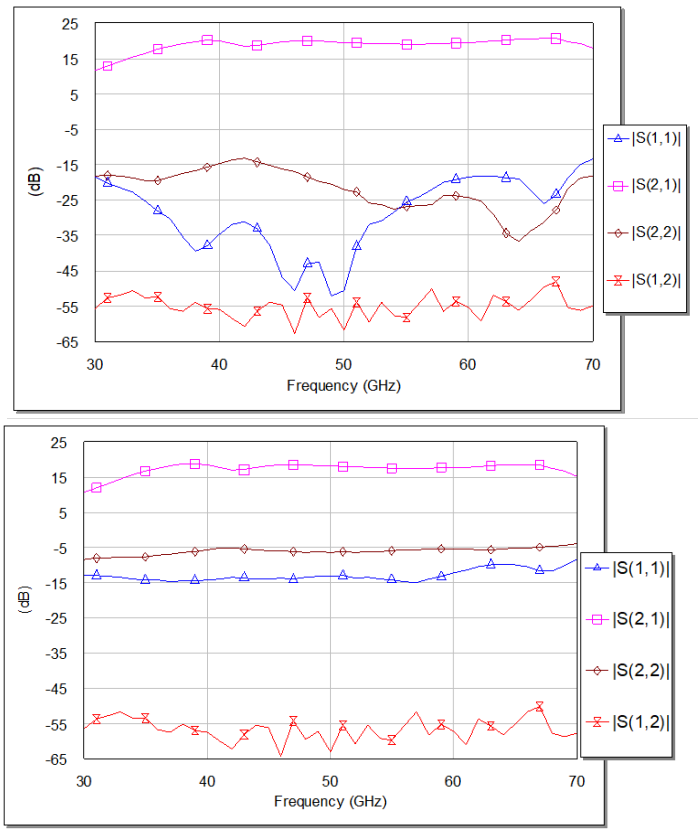

Figure 3.19: a) The upper figure shows the theoretical parameters simulated in AWR, b) The lower figure shows the theoretical parameters with bonding effects simulated in AWR.

In order to measure the saturation power and gain of the amplifier, it is important to design a setup capable of protecting the PXA Signal Analyzer (N9030A) so that the output power is not greater than 30 [dBm], which would damage the equipment.

Figure 3.20 shows the experimental used setup, where an input power is generated with the signal generator (Anritsu MG36944c) between 20 and 25 [GHz] which is later multiplied *times* 2 to characterize the amplifier between 40 and 50 [GHz]. Subsequently, this signal is amplified to compensate the losses in the setup components. Then this signal is received by the power amplifier HMC1144 which operate depending on the configuration of the gate and drain voltages set with the DC source (Keithley model 2612A). The output power of the amplifier is attenuated in order not to exceed any case 30 [dBm], and finally, the output signal is measured with the PXA.

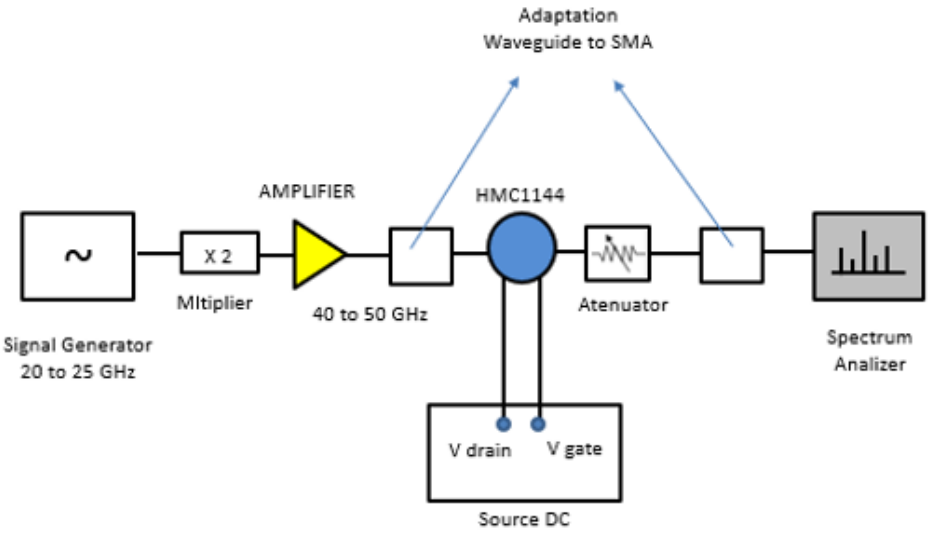

Figure 3.20: Setup scheme to measure the amplifier saturation.

The first configuration point was chosen according to the nominal parameters given by the datasheet, these are 4[V] of Drain. The second configuration point was chosen because it was in which a greater gain was obtained when characterizing the amplified with the VNA.

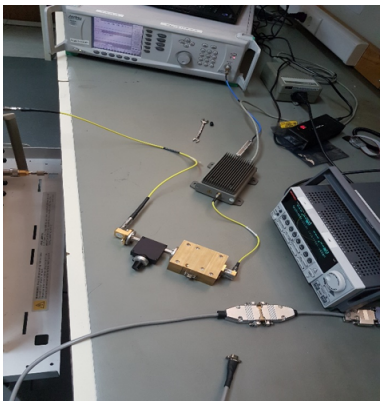

Figure 3.21: Setup photo to measure the amplifier saturation.

Table 3.2: configuration parameters for the operation of the MMIC.

Parameter	first configuration	second configuration
V drain (V)	5.6	3.5
V gate (V)	-0.56	-0.35
I drain(mA)	320	330

Once the drain and gate parameters were set, an input power was delivered with the signal generator and with the output power, the gain for the different input power values were calculated.

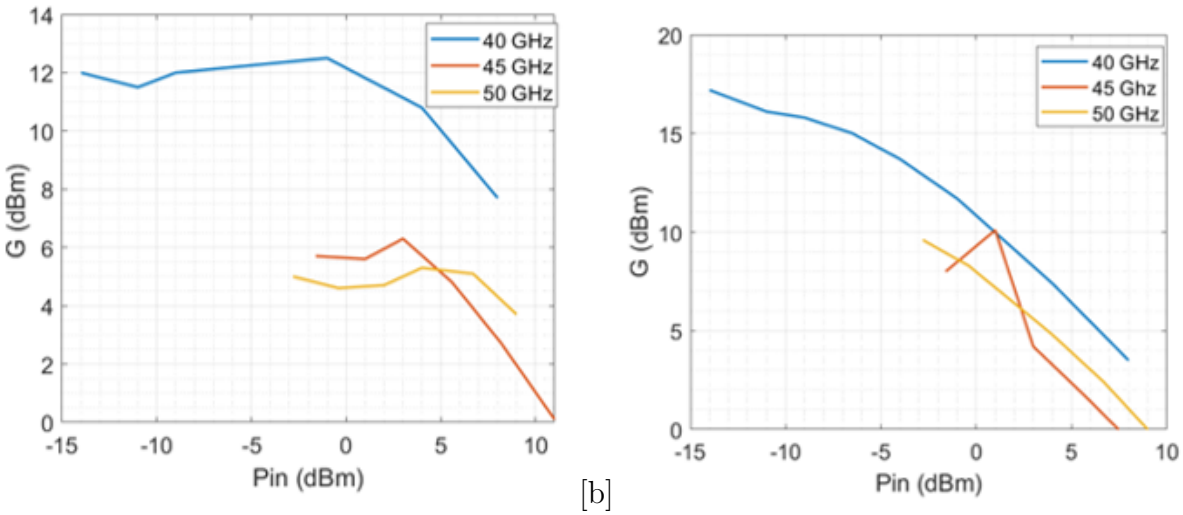

[a] [b]

Figure 3.22: a) Experimental gain vs. input power for the first configuration. b) Experimental gain vs. input power for the second configuration.

Figure 3.22 a shows the gain values for the nominal configuration. It is possible to observe that the gain remains generally constant for low values of the input power operating in the linear regime of the amplifier, and when the input power is greater than certain value, the amplifier enters the saturated state for which the gain begins to decrease.

This saturation effect is clearer in the second configuration, figure 3.22 b because the gain is greater for this configuration. The tendency of the decrease in the gain is clearly observed when increasing the input power, verifying that the amplifier is in the saturated state.

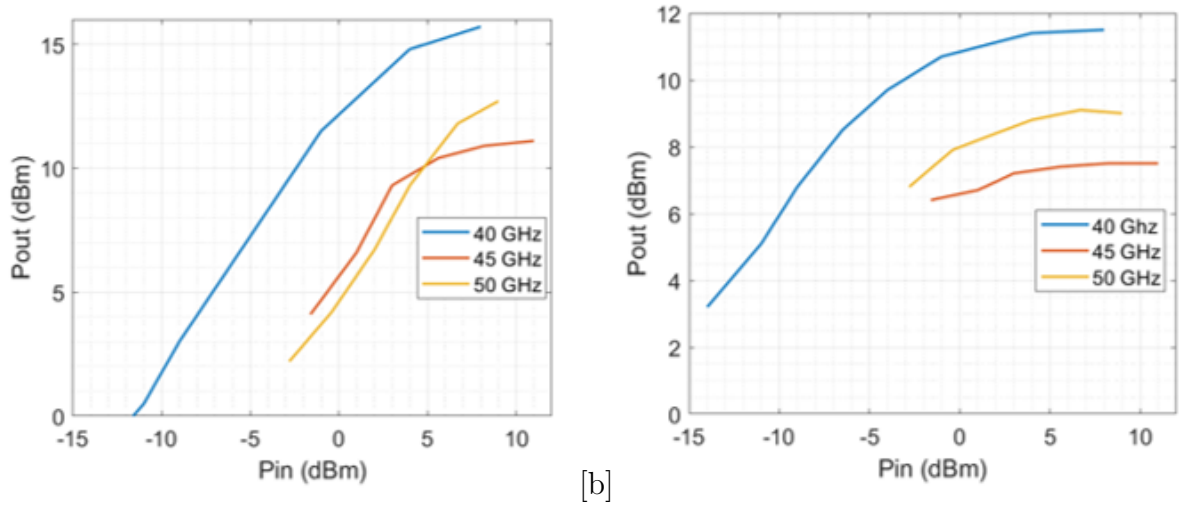

[a] [b]

Figure 3.23: a) Experimental output power vs. input power for the first configuration. b) Experimental output power vs. input power for the second configuration.

Analyzing the figures 3.22 and 3.23, it is also possible to observe that the nominal configuration obtains a greater output power at a higher input power. This is mainly due to two factors. The first factors is that the gain for this configuration remains constant when being

in the linear regime. The second factors is because when the input power is increased, the amplifier starts consuming a greater DC power, which is converted to RF power.

3.5 New Design

An improved version of the amplifier was designed in order to reduce the losses measured experimentally produced by the length of the bondings, the length of the waveguide, the number of bondings needed, and the number of microstrips. This also reduces the size of the unit by unifying the microstrip waveguide transition to the block for the chip.

The final design of the microstrip waveguide adaptation was made in the HFSS simulator, for which the same substrate duroid 5880 dielectric was used. The majority of the parameters were varied, decreasing as much as possible in order to reduce the size of the final block. The final parameters are presented in table 3.3.

Table 3.3: Valor parameters final design to the final block.

Parameter	mm
L	6.5
Ra	3
Lc	3
Ld	8.36
Lt	14
Li	11.888

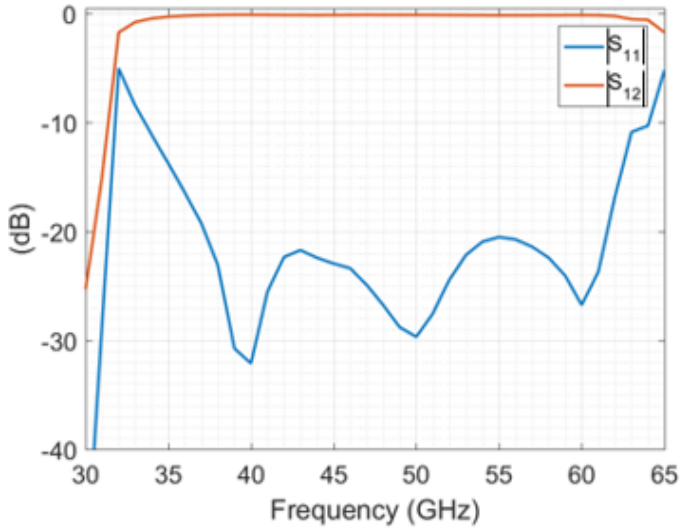

Figure 3.24: Final simulation results in HFSS For the optimized transition. The red curve represents the transmission coefficient and the blue curve blue the reflection coefficient.

The results of the simulations of the new design are presented in figure 3.24. The reflection coefficient is lower than -20 [dB] over the complete bandwidth, satisfying the design requirements of the transition. Later, a new mechanical design was carried out including the new transitions.

After importing the transition, the design was modified by adding the cavity required for the chip, the protection circuits, and the decoupling capacitors, obtaining the final design shown in figure 3.25.

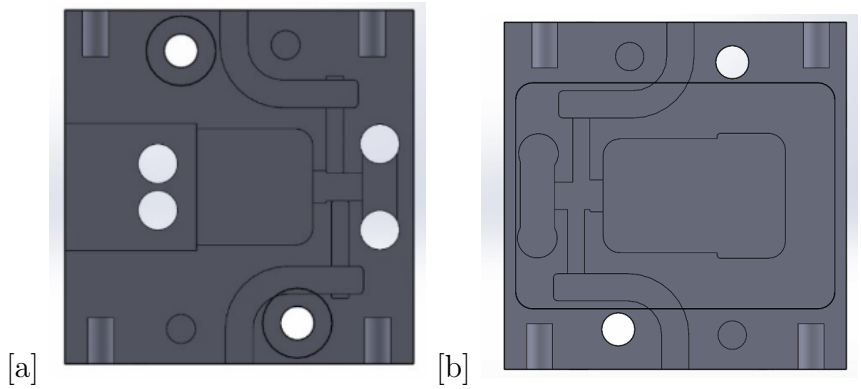

Figure 3.25: a) Final block design lower view. b) Final block design top view.

In order to reduce the space of the block, a cavity was done in the rear part of the block used to place the 4[V] protection circuit, as show figure 3.26 a. And the figure 3.26 b show the cover to close this later.

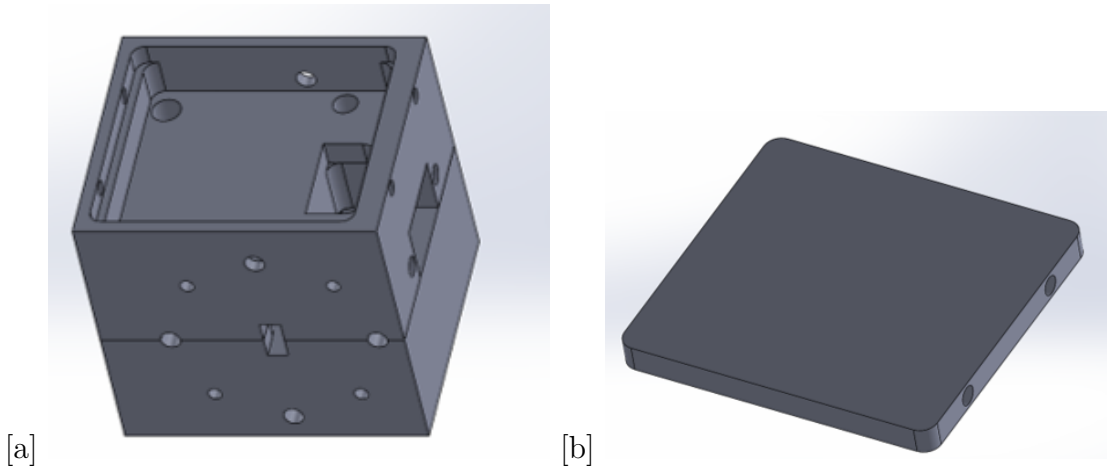

Figure 3.26: a) Rear view of the lower block designed in Solidworks. b) Cover designed in Solidworks.

The new design allows reducing the need for bonding between the transition blocks and the block for the chip. It also reduces the size and weight considerably as shown figure 3.27 and table 3.4. This block is currently in the process of manufacturing.

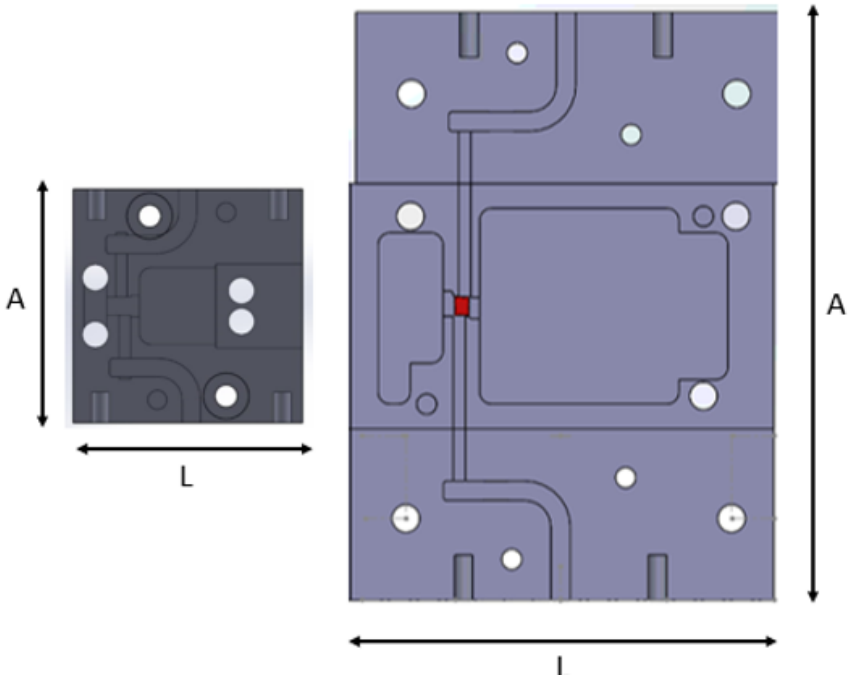

Figure 3.27: In the figure on the left it is possible to see the bottom view of the final design, and on the right of the initial design.

Table 3.4: Valor parameters final design to the final block.

Design	L[mm]	A[mm]	H[mm]
First	52	72	30
Second	30	30.4	32

3.6 Conclusion

In this chapter we have designed, manufactured and characterized a power amplifier based on the integrated circuit HMC1144 that operates in the WR19 band (39,2-59,6 [GHz]). Initially, a microstrip waveguide transition was designed based on a radial antenna design to obtain reflections below -20 [dB]. Subsequently, this design was exported to Solidworks to make the design of a transition block.

Once the microstrip waveguide transitions were fabricated, the transmission coefficient measurements were done back to back, observing that on average between 35 to 50 [GHz] there is approximately 2,2 [dB] of loss. Later, the biasing circuit of the MMIC, the voltage protection circuits, the 50 [Ω] transmission lines to connect the input and output of the amplifier with the transition block with the RF signal, were designed.

After designing the block, it was built with a CNC machine, to later mount the protection circuits, the 50 [Ω] lines, and the chip in it. The electrical connections were made using the bonding machine. Once the components were mounted on the support block, the waveguide to microstrip transition blocks were connected to it, and the gain obtained was measured using the Vector Network Analyzer (VNA). The experimental measurements obtained show that the gain does not match the values delivered by the manufacturer, lower values of gain were obtained. This can be attributed to the losses in the transition back to back which was measured experimentally. Another factor of importance is that the length of the bodings was larger than the recommended value. The effect of the bond length was simulated in AWR showing a loss greater than 2 [dB] over the entire bandwidth.

The characterization of the amplifier shows a gain $|S_{21}|$ over 15 [dB] between 35 to 41 [GHz] and at higher frequencies, but its gain drops significantly to approximately 13 [dB] between 43 to 50 [GHz].The reflection coefficient $|S_{11}|$ is less than -10 [dB] between 35 to 42 [GHz] and about 47 [GHz], but in the rest of the band increases about -8 [dB].

The performance of the equipment in saturation was also characterized in two different configurations, one with the nominal parameters given by the manufacturer, and the other was chosen because it allowed obtaining a greater gain.

The results show for the nominal configuration that the gain remains constant 12 [dBm] for low values of the input power (linear regime of the amplifier), and when the power input is greater than a certain value, the amplifier enters the saturated state in which the gain begins to decrease. The value of the saturation point depends on the frequency of work. For the second configuration, the saturation effect is clearer because the initial gain is greater for this configuration approximately 17 [dBm]. The tendency of the decrease in the gain is clearly observed when increasing the input power, verifying that the amplifier is in the saturated state.

A new block was designed in order to reduce the losses measured experimentally and reduce the size of this by unifying the microstrip waveguide transition to the block for the chip and decreasing the bonding length.

Chapter 4

EQUALIZER

To compensate the weak signals received by the receivers, low-noise amplifiers (LNAs) are commonly used, such as the CGY2190UH / C2 amplifier[0]. However, the LNA-type amplifiers have a maximum gain in the lower band and decay around 5 [dB] at higher frequencies[0]. These drawbacks can be resolved by using a gain equalizer, which can compensate for the attenuation in the upper band. In this chapter, microstrip branches and thin-film resistors were used to design a microwave gain equalizer. The equalizer was designed to work in the W band. The required equalization value is approximately 5 [dB][0].

4.1 Introduction

The equalization value is defined as the maximum attenuation and the minimum attenuation difference. It is possible to determine the attenuation curve with the fluctuation of the gain of the amplifier. To create an equalizer, the design can be based on a typical RLC resonator, tuned to operate on a certain frequency w_0, showing a form to a "bell", as shown in the figure 4.1.

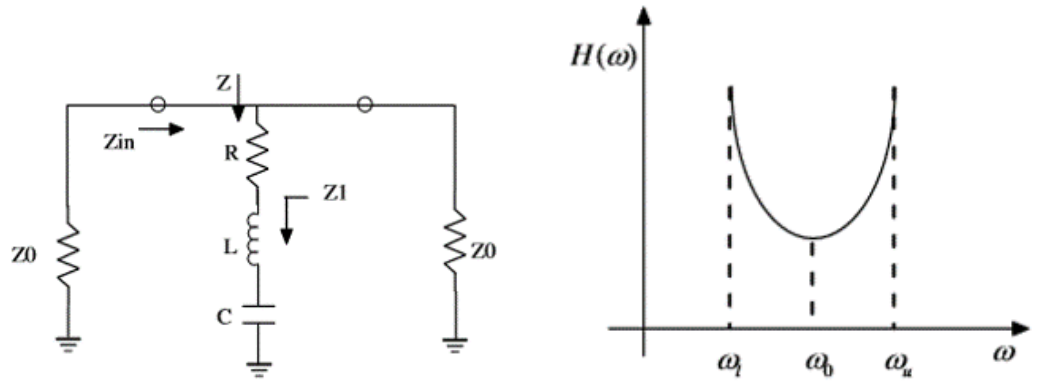

Figure 4.1: a) RLC resonator scheme in series. b) Frequency response of resonator RLC in series in bell shape. Taken from [0].

The cascaded connection of several resonators in series allows a convenient modification of the frequency response. Carefully choosing the resonance frequency of each resonator, it is possible to obtain a gain slope to compensate for the attenuation produced in the LNA [0]-[0].

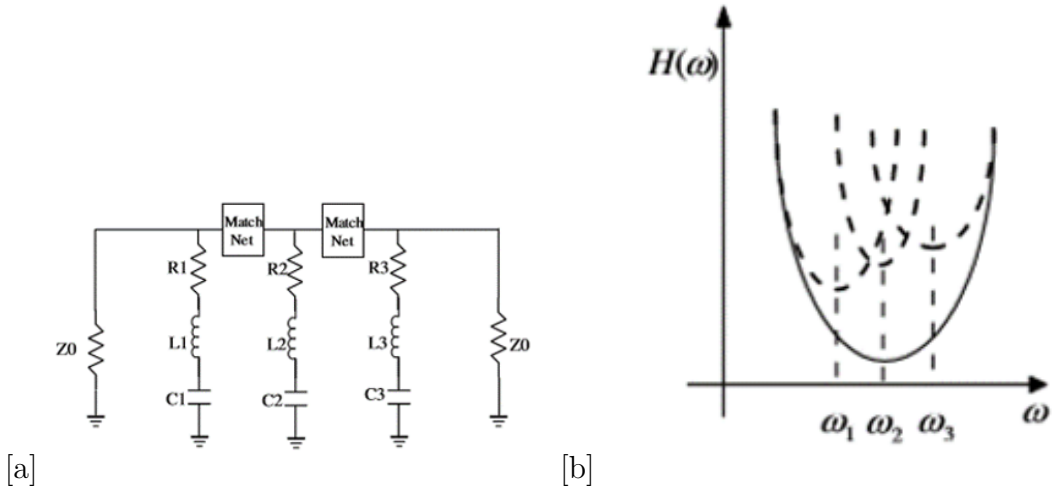

Figure 4.2: a) Cascade circuit model. b) Frequency response of resonators Taken from [0].

Once the desired slope gain for the equalizer is obtained, it is preferred to work with microstrip lines instead of an RLC circuit because of its easier fabrication. This is possible because a terminal open line of quarter wavelength can be equivalent to an RLC series resonant circuit [0].

For the design of the equalizer, the dielectric Duroid 5880 was used. This dielectric is 0.127 [mm] thick and its relative constant is 2.2. The AWR simulator to compare the behavior of the gain slope for different number of resonators, as seen in figure 4.3.

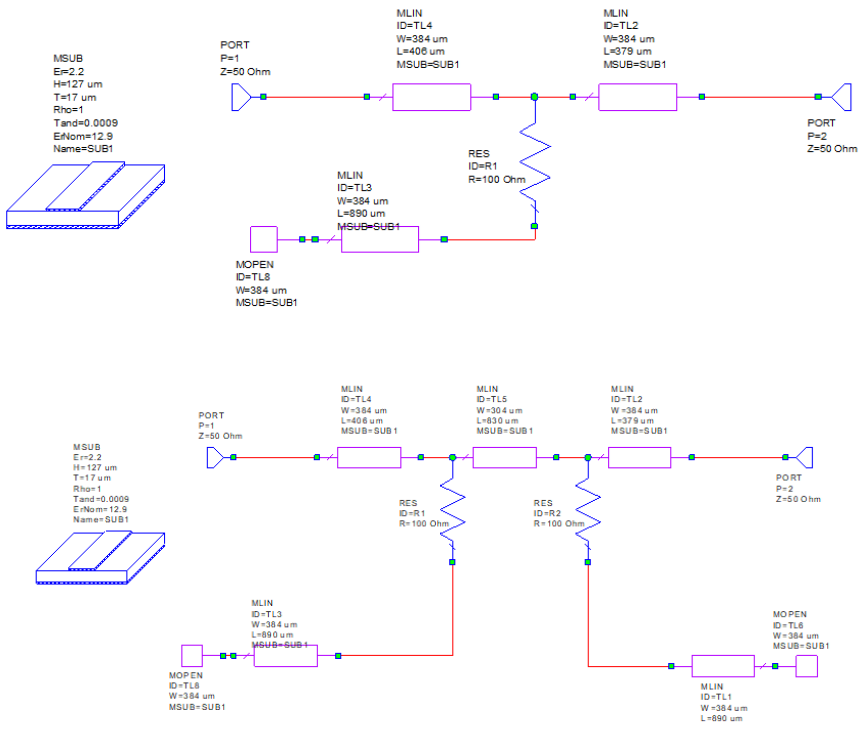

Figure 4.3: Schematics of basic circuits of resonator in AWR. a)The upper figure shows one resonator. b) The lower figure shows two resonators.

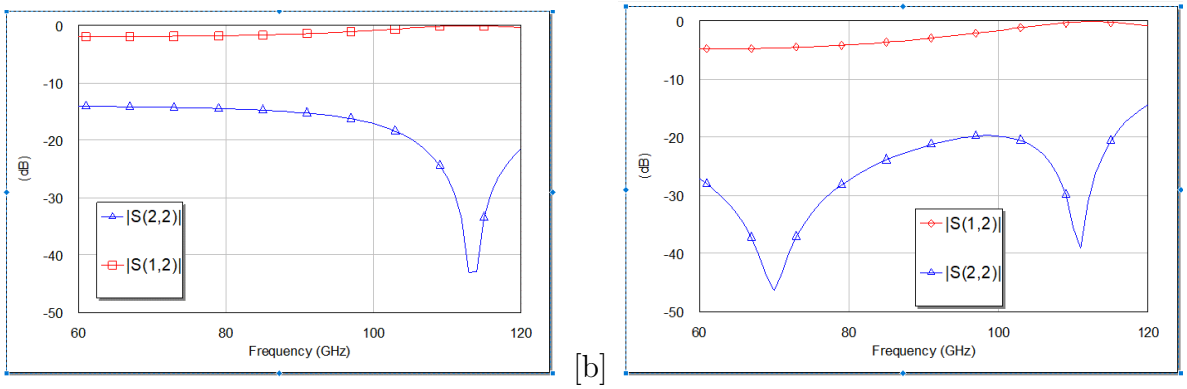

Figure 4.4: Frequency responses of basic circuits of resonator in AWR. a)One resonator. b) Two resonators.

4.2 Design of a Microstrip Gain Equalizer

From the simulations realized in AWR figure 4.4, it was possible to observe that we obtain a greater gain slope if we increase the number of resonators. However, this also increases the size of the resonator, as seen in the figure 4.3. Therefore, the number of resonators must be chosen to compensate slope gain, and the smallest possible size.

Due to mechanical restrictions and requirements, the equalizer consists of two open terminal lines. To reduce the reflection coefficient, some adaptation lines should be added at the input and output ends. A simulated AWR model of equalizer gain is shown in the figure 4.5.

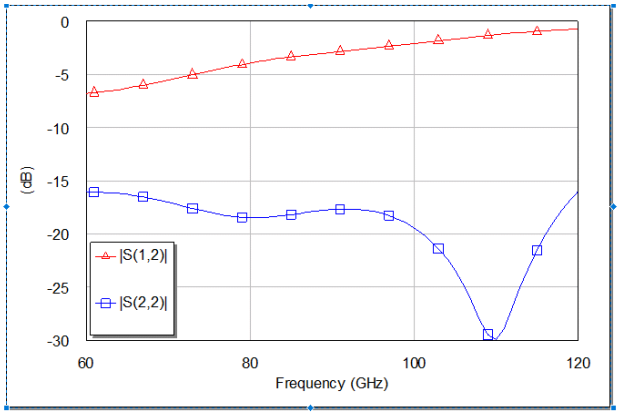

Figure 4.5: Initial equalizer frequency response to simulation in AWR.

This figure shows an optimized equalizer based on two cascaded resonators obtain a gain slope greater than 5 [dB]. However, because of the width of the circuit, it can not exceed 1 [mm] by mechanical manufacturing constraints, a new design was chosen based in two resonators coupled, as shown the figure 4.6. However, AWR is not able to simulate the effect of two resonators coupled, it is for this reason that a second design was done using HFSS.

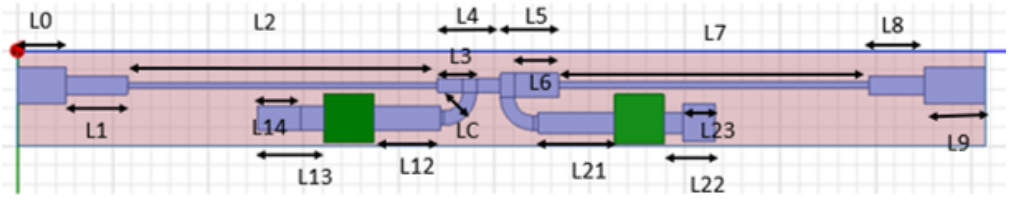

Figure 4.6: Final equalizer design in HFSS. The green blocks correspond to the resistances.

The new design performed in HFSS delivers more precise solution since it is based on fully solving Maxwell equations in three-dimensional space. Figure 4.6 shows the schematic of an optimized resonator design and figure 4.7 the corresponding frequency response. In table 4.1 it is possible to review the length and width parameters for each line used.

Table 4.1: Parameters the final equalizer.

N	W (um)	L(um)	N	W (um)	L(um)
0	60	510	9	60	580
1	60	645	12	60	700
2	60	3250	13	60	600
3	60	260	14	60	450
4	60	250	21	60	800
5	60	150	22	60	530
6	60	450	23	60	330
7	60	3250	C	150	350
8	60	291	Ltotal	-	10000

Through the HFSS simulation, we found the frequency of the resonators and the associated quality factor changing the dimensions of the microstrip. The resistances were fixed to 100 [Ω]. We obtained an equalization value of approximately 4.3 [dB] in the entire W band and a maximum equalization of approximately 8 dB between 73 to 110 [GHz]. This model was made considering that the maximum width of the circuit should be 1[mm].

Because adaptation lines were added to the equalizer and the thin film resistance, the input reflection coefficient is lower than −10 [dB], consisting with our design objectives.

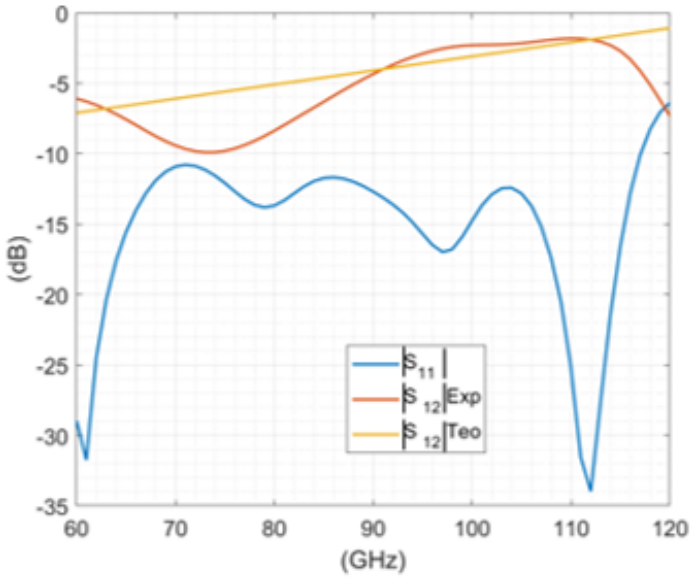

Figure 4.7: Equalizer frequency response to simulation in HFSS. The red color is the transmission coefficient curve, and the blue color is the reflection coefficient curve.The orange color is the desired transmission coefficient curve, with a slope of 0.1 [dB]

4.3 Conclusion

In this chapter, a microwave gain equalizer for the W band 67-117 [GHz] was designed. It uses 2 microstrip resonator branches with an integrated thin film resistor. From the designs, it was possible to observe that as more resonators are used, higher equalization. However, the final design consists of 2 resonators in order to achieve the smallest possible size to integrate this into our down conversion module.

The equalization value obtained by simulations was approximately 4.3 [dB] in the entire W band and a maximum equalization of approximately 8 [dB] between 73 to 110 [GHz], which is within the required values [dB]. Although an equalization of 5 [dB] was desired, this is not possible to achieve across the bandwidth due to mechanical design impediments. The characteristics of the designed equalizer compensate for the loss obtained at high frequencies with the low noise amplifiers. Therefore, this design will be taken as a base for the manufacturing of the equalizer in the laser LPKF printer of the Millimeter Wave Laboratory.

Chapter 5

EDGE COUPLED MICROSTRIP BANDPASS FILTER FOR THE W BAND

Filters are an important component in any radio frequency system because they allow to select signals within a specific bandwidth around a central frequency. Morever, they reject signals in another frequency range, which have the potential to interfere with information signals [0] - [0]. In our case we will use a subharmonic mixer to down convert the RF signal to the IF band. The process includes the generation of several intermodulations producing the mixture of RF frequency components and an integer multiple of LO frequency, so the filter becomes fundamental to eliminate the unwanted components.

In this chapter, we describe the design and simulation of an edge coupled microstrip filter to obtain bandpass filters with Chebyshev response. We have selected this type of filter because it has a more abrupt fall of the gain outside the pass band than other filters such as Bessel and binomial[0]. However, it has the disadvantage of a ripple in the pass band. The initial design was made in AWR and later in HFSS. The bandpass filters was designed to work in the W band.

5.1 Introduction

As technologies advance, stricter filter requirements are required. One of the requirements is compactness. At very high frequencies, practical inductors and capacitors lose their intrinsic characteristics so, for microwave frequencies ($>$ 3GHz), filter are normally made using distributed elements, such as transmission line sections [0] [0]. It is also possible to find waveguides filter used at higher frequencies. However, waveguide systems are bulky and expensive [0]. More economical alternatives to higher frequencies are stripline and microstrip filters. These transmission lines are compact, low-cost manufacturing, permit easy integration, and its design is relatively simple [0] [0].

A microwave filter is a linear, passive, reciprocal, two-port device that strongly attenuates

unwanted signal frequencies while allowing the transmission of the desired frequency. In general, the electrical performance of the filter is described in terms of insertion loss, return loss and frequency selectivity.

The frequency range through which a bandpass filter has a transmission coefficient near unity is called the passband. Due to its easy integration and its compact designs the coupled line structure has become a popular choice of architecture for microstrip bandpass filter. The architecture shown in figure 5.1 is of a general design of a bandpass filter composed of a cascade of coupled line sections N + 1 (the sections are numbered from left to right).

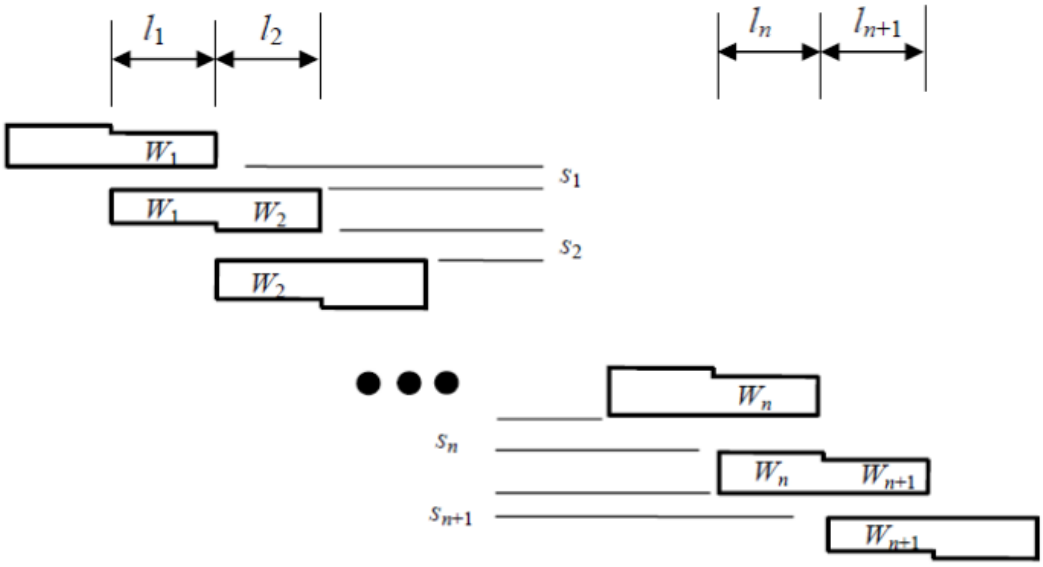

Figure 5.1: Bandpass filter structure[0].

The filter structure consists of a circuit of coupled transmission lines. The coupling spaces correspond to the admittance inverters in the prototype low-pass circuit. The characteristic impedance of even and odd modes of the half-wave resonators coupled in parallel are calculated using admittance inverters. These impedances of even and odd mode are then used to calculate the physical dimensions of the filter[0]. Each section of the filter contains three parameters: S, W and T. Two ribbon lines of W width are in the configuration parallel or coupled to the edge with a separation S and T the height of the substrate[0].

5.2 Design of bandpass filter 1

The initial design was made using the filter wizard from Microwave Office (AWR). Table 5.1 presents the technical specifications.

Table 5.1: Filter 1 design specifications to print in the Laser Printer LPKF.

Characteristic	Specifications
Filter response	Chebyshev
Center frequency	95 [Ghz]
Operating range	67 to 116 [GHz]
Bandwidth	60 [GHz]
Ripple	0.1 [dB]
Min. W	60 [um]
Min. S	60 [um]
Source Impedance	50 [Ohms]
Substrate	Duroid 5880
Thickness of substrate	127 [um]
Dielectric Constant	2.2

For the design of the Filter, the dielectric Duroid 5880 was used. This dielectric is 0.127 [mm] thick and its dielectric constant is 2.2. The width W and the space S between the tracks were chosen according to the resolution of the LPKF laser printer of the Millimeter Wave Laboratory.

Once the design parameters and mechanical restrictions were specified in the Filter Wizard, we simulated the behavior of filters of different order. An order 7 filter was chosen because it presented a lower insertion loss and a better attenuation outside the band of interest than the filters of order 6 and 8 simulated. It also presents a good physical size.

Figure 5.2 presents the results obtained from the simulation carried out in AWR. It is possible to observe that the return loss $|S_{11}|$ is lower than -10 [dB] in most of the band with a degradation at the edges. Additionally, the parameter of insertion loss $|S_{21}|$ is less than -0.5 [dB] around the center frequency but presents larger attenuate at the ends of the band.

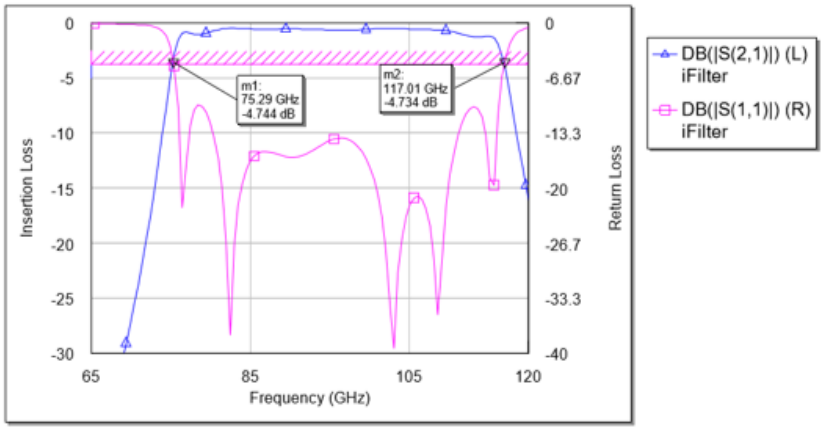

Figure 5.2: Frequency response filter 1 simulated in AWR.

Based on the preliminary design carried out in AWR, a second design optimization was performed in HFSS, obtaining the final design shown in figure 5.3 The final parameters are presented in table 5.2.

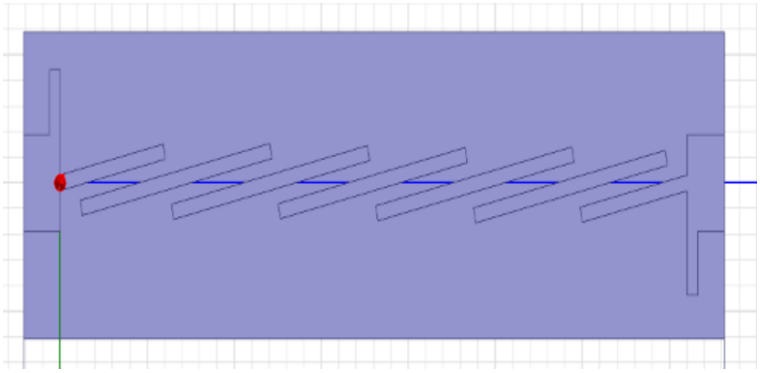

Figure 5.3: Layout of the proposed 7th order filter 1 design in HFSS. The design presents an inclination on the coupled lines to obtain aligned inputs and outputs.

Table 5.2: Filter 1 parameters.

N	W (um)	S (um)	L(um)
1	60	60	530
2	60	60	560
3	60	60	590
4	60	60	544
5	60	60	600
6	60	60	518

Figure 5.4 shows the results obtained from the design of the filter made in HFSS. This design does not give us a better result than the one obtained in AWR. The return loss $|S_{11}|$ is lower than -10 [dB] in most of the band, but not in the whole as desired. The insertion losses $|S_{21}|$ are greater than -1 [dB] around the center frequency, except at the edges.

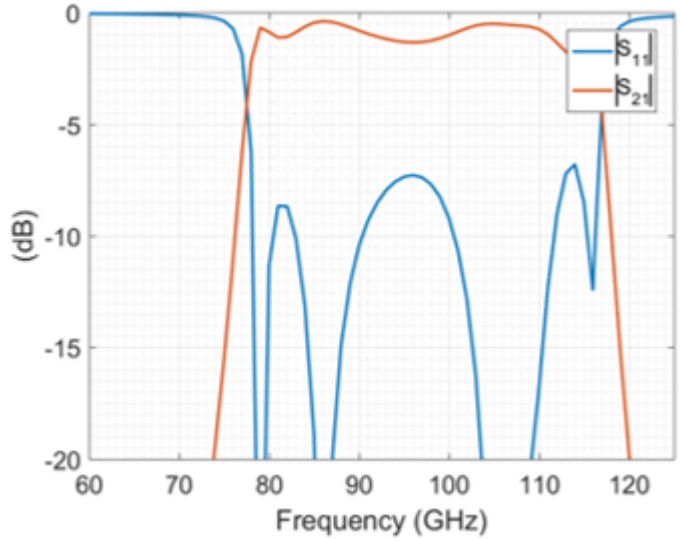

Figure 5.4: Frequency response filter 1 simulated in HFSS.

A good bandpass filter requires a low insertion loss in its passband, as well as a narrow passband with the highest possible attenuation out of the Band. It also needs a great return loss for a good adaptation of the impedance with the interconnection components and a high-frequency selectivity to avoid interference. Our first design does not meet these requirements. The main reason is that the mechanical restrictions imposed on the widths of the tracks and the spaces between them are taken not less than 60 [um]. The reason is that when working at a higher frequency, the wavelength is smaller, which is directly related to the design parameters. To solve this problem, was decided to change the manufacturing methodology and implement the filter this through the company Ion Beam Milling who are able to design filter with lines and spaces as small as 10 [um] and controlled to tolerances of 1 [um] in substrate of quartz.

5.3 Design of bandpass filter 2

With the new design specifications delivered by the company Ion Beam Milling, we proceeded to work with the AWR simulator to compare the behavior of filters of the different order.

Table 5.3: Filter 2 design specifications to print in the Laser Printer LPKF.

Characteristic	Specifications
Filter response	Chebyshev
Center frequency	95 Ghz
Operating range	67 GHz to 116 GHz
Bandwidth	60 GHz
Ripple	0.1 dB
Min. W	10 um
Min. S	10 um
Source Impedance	50 Ohms
Substrate	Polished Fused Silica (Quartz)
Thickness of substrate	127 um
Dielectric Constant	3.8

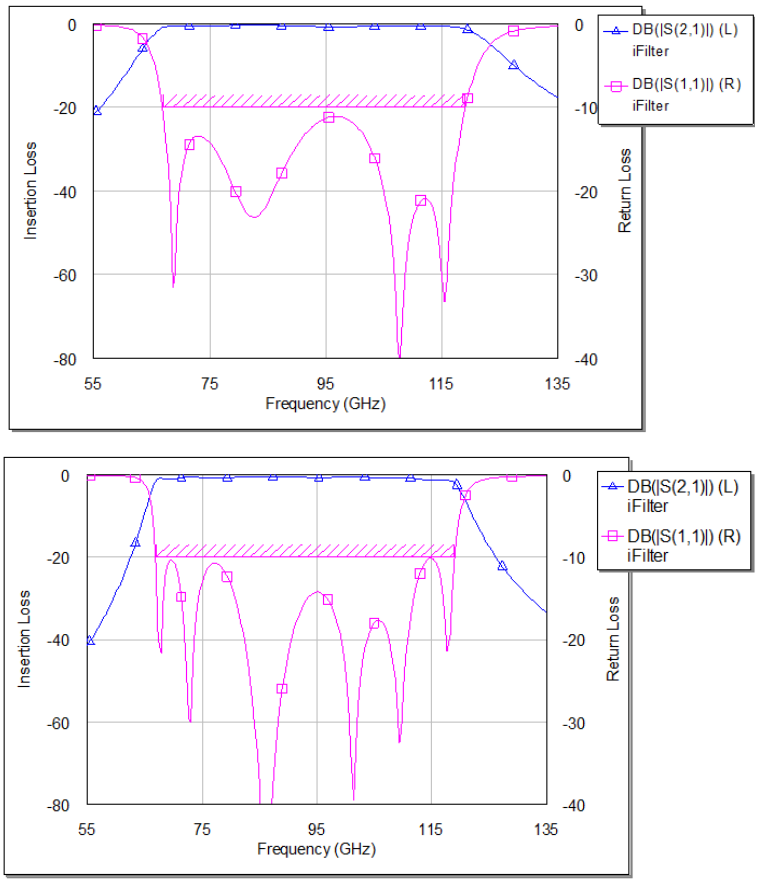

Figure 5.5: The upper figure shows the frequency response the filter of order 5 simulated in AWR. The lower figure shows the frequency response the filter of order 7 simulate in AWR.

It was possible to observe through the AWR Filter Wizard, that both a filter of order 5 and one of order 7, are able to achieve return loss less than -20 [dB] in the whole bandwidth, and losses by insertion less than -1 [dB] in almost the entire bandwidth except at the edges. Higher-order filters may have a narrower form factor but will be a physically larger. Finally, the 7th order filter was chosen.

To obtain a better control of the parameters, the final optimization of the filter was done in HFSS.

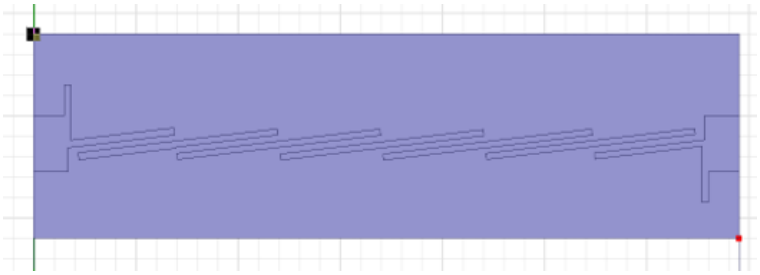

Figure 5.6: Layout of the proposed 7th order filter 7 design in HFSS.

Table 5.4: Filter 2 parameters.

N	W (um)	S (um)	L(um)
1	35	30	480
2	30	31	501
3	30	33	500
4	30	30	500
5	30	27	528
6	29	33	500

Figure 5.7 shows the obtained results. The return loss $|S_{11}|$ is less than -12 [dB] in almost the entire bandwidth between 72 to 117 [GHz], except in the lower part of the band where it is less than -9 [dB]. The insertion loss $|S_{21}|$ are approximately less than -1 [dB] in the entire operating band, and outside of it rapidly decays to -15 [dB] under 60 and over 125 [GHz], as desired.

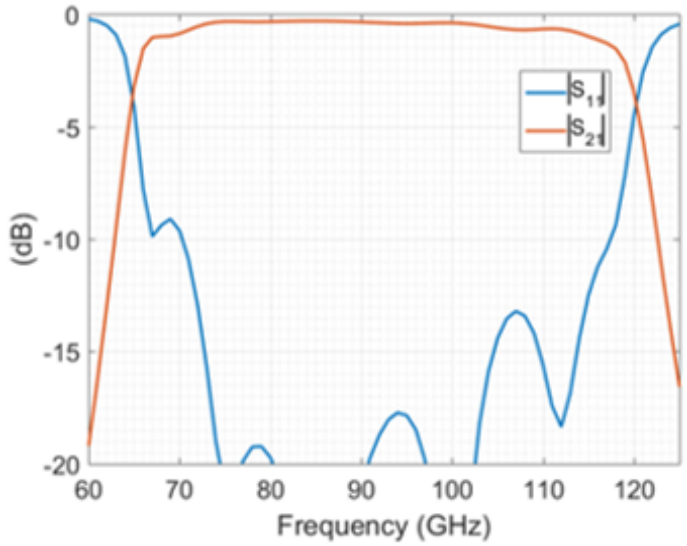

Figure 5.7: Frequency response filter 2 simulated in HFSS.

5.4 Conclusion

We have described a procedure for the design of a bandpass filter for the W band. The filter consists of coupled transmission lines, based on the Chebyshev approach. Two designs were made; the first consists of a 7th order filter manufactured in Duroid 5880 with restrictions imposed for the manufacture subsequent. This means that the width and the separation of the tracks should not be less than 60 [um]. This first design did not achieve the objectives; because the return loss $|S_{11}|$ is less than -10 [dB] only in some frequencies, but not in the whole band as desired.

Due to these problems, a second filter was designed. This filter uses quartz as substrate and will be manufactured in Iom Beam Milling, which presents more flexibility for the design. This design allows the width and the separation of the tracks to be smaller than the first design, but not less than 10 [um], and tolerance up to 1 [um]. The second design allows the reduction of the return loss to less than -12 [dB] between 72 to 117 [GHz]. In the lower part of the band (less than 72 [Ghz]), the return loss is less than -9 dB. This also shows good insertion loss, fulfilling the desired objectives.

Chapter 6

LANGE COUPLER

Chapter 2 described the advantages of the 2SB configuration over other configurations, and the need to use a hybrid or lange coupler. This component allows separating the RF signal into two identical signals by reducing its power by -3 dB and adding a 90° phase shift between the outputs.

Currently, it is possible to find a large number of publications on integrated coupled lines, called lange coupler [0]-[0]. Hybrids used to be the most popular option in phase changes, but lange couplers could potentially replace them. This is because a Lange coupler allows the design of a circuit with lower economic cost, that is easier to manufacture and that is more compact.

Designing a mixer based on a lange coupler has the disadvantage that the rejection of the lateral band depends to a large extent on the amplitude and the phase imbalance of the whole system [0]-[0]. To minimize the imbalance, the total electrical length and gain must be the same in the two branches of the system.

In this chapter, we will present the design of a lange operating in the W band.

6.1 Introduction

The interdigitated directional coupler, invented by Dr. Julius Lange around 1969, has become a popular element in unilateral microstrip circuits [0]-[0]. The design procedure for the Lange coupler requires a numerical solution for the capacitance distribution in a system of N equal conductors. The Lange coupler is an interdigited four-port structure, which is widely used for the design of combiners and RF power dividers, as well as in mixers and modulators. The coupling is derived from transmission lines with a conductor of width W, a small spacing S, and the thickness t, such as microstrip lines. Normally, the number of conductors (N) is even. In figure 6.1 it is possible to observe the typical geometry for a Lange coupler of $N = 4$ [0]-[0].

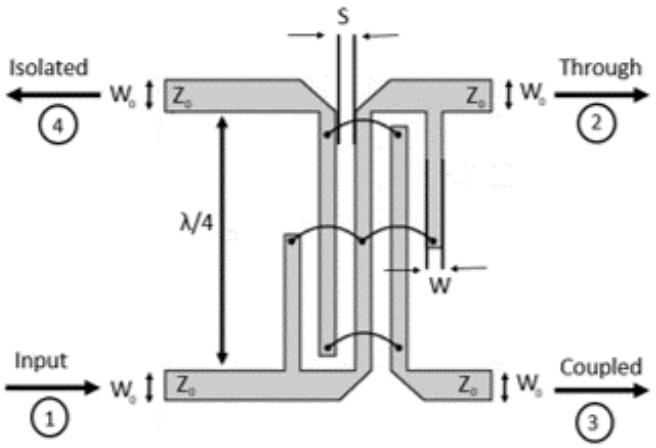

Figure 6.1: Schematic of Lange coupler[0].

Figure 6.1 shows the general diagram of a lange coupler. The power is injected at the input port (1) and then coupler equally splits the incident power to the through (2) and coupled (3) ports with the 90° phase difference. Isolation port (4) is internally terminated with the match load so as to eliminate the reflected power because of mismatches [0].

The length L is established by the desired center frequency $|f_0|$, and must be equal to the quarter of the wavelength λ_s:

$$L = \frac{\lambda_s}{4} \tag{6.1}$$

λ_s is represented by the following equation:

$$\lambda_s = \frac{c}{f_0\sqrt{\varepsilon_{eff}}} \tag{6.2}$$

ε_{eff} is the effective dielectric constant, which is a function of the dielectric constant of the substrate, the thickness of the dielectric h, the width of the conductor W and the thickness of the conductor t. The response of the Lange coupler is very sensitive to the change of its variables S, W and h because they allow finding the characteristic impedances of the even and odd modes. The other parameters involved are the width of the bonding and the width of the conductor of the input tracks W_0 as shown in figure 6.1. The width W_0 of the conductor must be selected such that for the characteristic impedance is close to 50 [Ω] [0]-[0].

An important factor when designing the Lange coupler is the imbalance of amplitude and phase. This can be understood from the the fact that the sideband rejection in the mixer is influenced by the amplitude and phase imbalance by:

$$R = -10 * log\left[\frac{1 - 2 * \sqrt{\Gamma} * cos\Theta + \Gamma}{1 + 2 * \sqrt{\Gamma} * cos\Theta + \Gamma}\right] \tag{6.3}$$

Γ, Θ are the amplitude and phase imbalances, respectively [0]. Figure 6.2 shows the influence of amplitude and phase imbalances on the rejection relationship. The lower the imbalance, the greater the rejection of the lateral band, as desired. Modern analog receivers achieve sideband rejections between 10 and 20 [dB] because it is very difficult to have a low imbalance. However this problem is now overcome by implementing a hybrid IF digitally, instead of a second lange coupler[0]-[0].

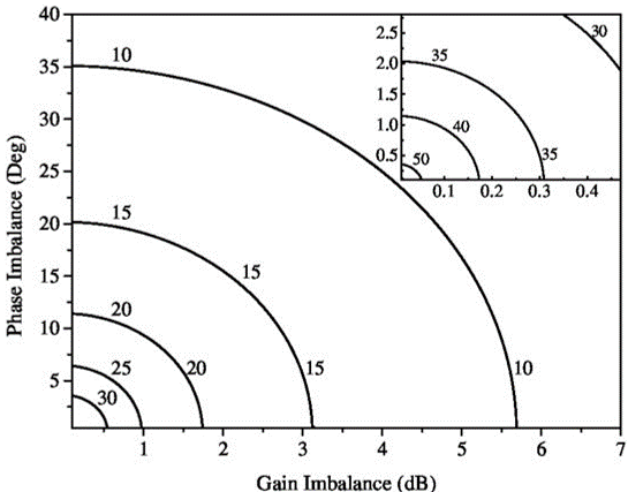

Figure 6.2: Effect of amplitude and phase unbalance in balanced mixers and sideband separators[0].

6.2 Design of Lange Coupler

Since AWR already has a computer program for the design solution of a Lange coupler, it will be used to obtain a first design with the following restrictions for the subsequent manufacture in Ion Beam Milling:

- Minimum distances of 10 [μm] between lines.
- The width of the copper lines 10 [μm].
- Minimum manufacturing precision 1 [μm].
- The height of copper lines 17 [μm].
- Dielectric to use Quartz, with dielectric constant equal to 3.8.
- Dielectric height 127 [μm].

Once the design limitations were defined, the lange coupler was designed, for which the AWR base design was re-centered around a central frequency of 90 [GHz].

Figure 6.3 shows the scheme of the initial design obtained through the AWR optimizer. Unlike the schematic shown in figure 6.1, in this design an impedance matching track was added between the inputs and outputs of the lange coupler and the microstrip of 50 [Ω] for later connection. The length and width values for microstrip lines were synthesized by using the TXLINE tool incorporated in the AWR software.

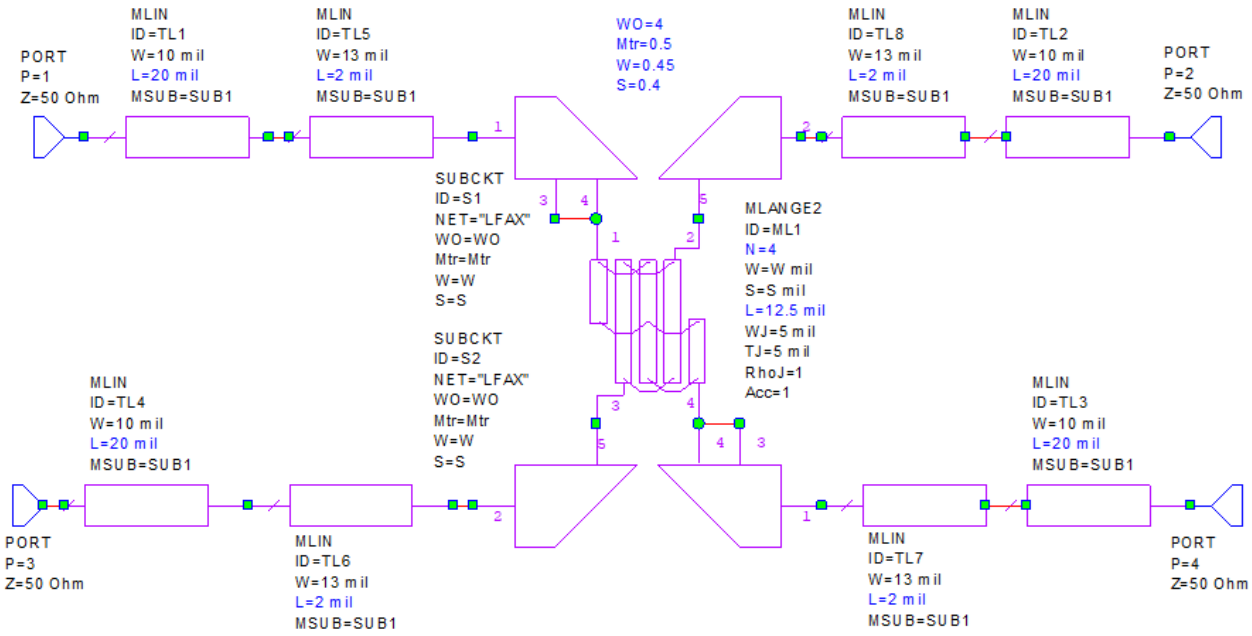

Figure 6.3: Schematic of lange coupler designed in AWR.

Figure 6.4 presents the frequency response of the S parameters of the designed lange coupler. From this, it is possible to observe that the isolation and return losses are around -7 at low frequency, but increase with the frequency to approximately -4.5 [dB]. It is also observed that if the relation s/h is maintained equal to approximately 0.1, and the ratio of width W to spacing S is in the range of 1 to 2, then the coupling is around -3 [dB] and independent of the variations in S, W, and h [0].

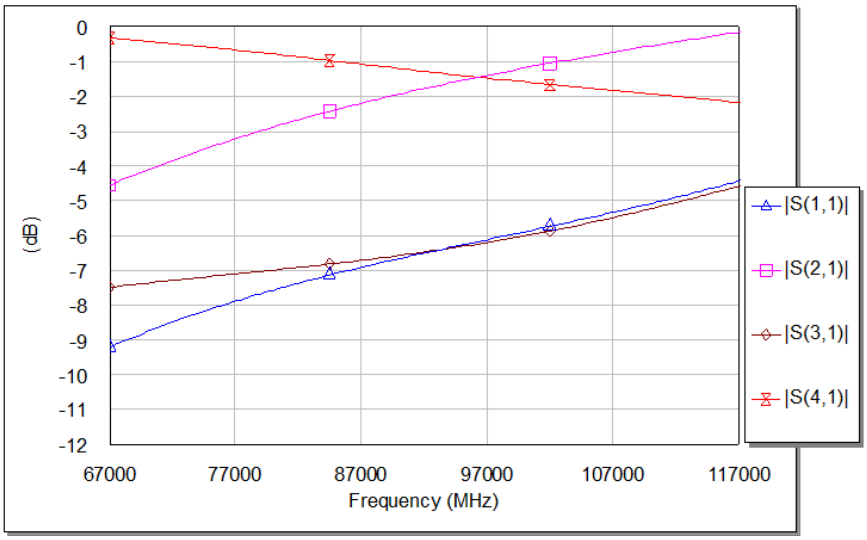

Figure 6.4: S-paramters versus frequency simulated in AWR.

For the final design, it is desired that the isolation and return loss are less -10 [dB] and that gain imbalance is lower in the whole band. Unfortunately, it was not possible to obtain these values with a first approximation in AWR. Neither was possible to obtain a design that matches the desired imbalance gain. Because imbalance gain presented good results only near the center frequency of the band.

In change, it was obtained a good phase imbalance as shown in figure 6.5, less of 5 degrees of phase imbalance in the whole bandwidth.

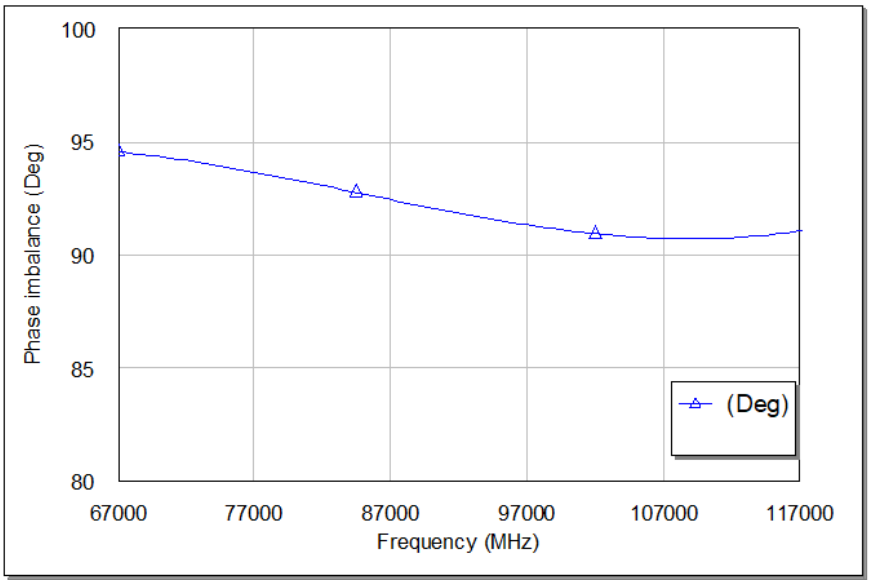

Figure 6.5: Imbalance phase versus frequency simulated in AWR.

Based on the initial design made in AWR, we proceeded to design and simulate the lange coupler in HFSS. The design is presented in figure 6.6, and its parameters in table 6.1.

Table 6.1: Parameters the lange Coupler.

Parameter	μm	Parameter	μm
L	380	L2	100
L0	380	W3	282
W	20	W4	254
S	10	L4	80
W0	100	W5	150
W1	70	L5	100
L1	250	W6	266
W2	200	L6	100

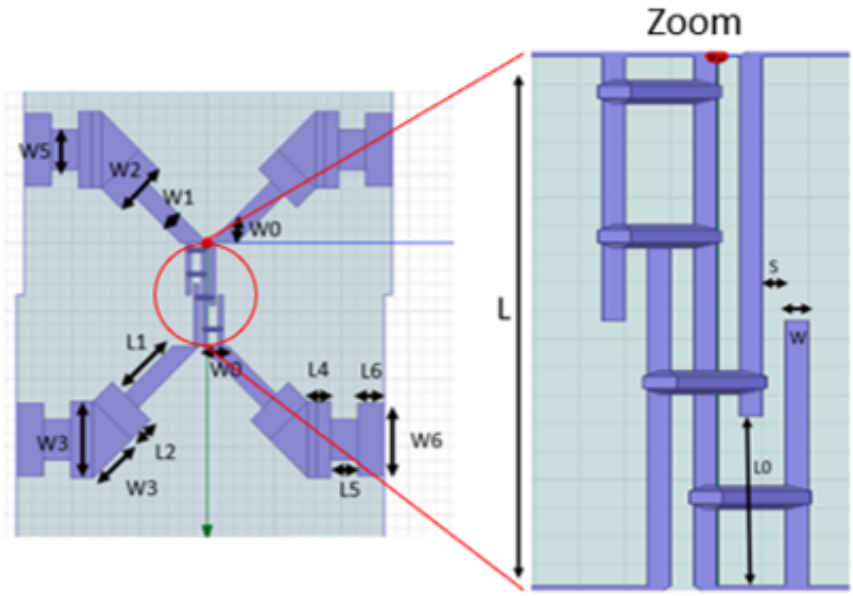

Figure 6.6: Schematic of lange coupler designed in HFSS.

The final design was based on the initial design in AWR, but it was necessary to make modifications to the dimensions of the width of the tracks because the diameter dimensions of the bondings are 18 [μm]. It is for this reason, that a minimum W=18 [μm] was imposed, what will allow makings the bondings correctly later.

Another important factor is the fact that when working with small dimensions coupling effects occur between the microstrip, which is not considered in the AWR model. It is for this reason that geometric modifications were made to the design, in order to eliminate the coupling effects.

The final results of the electromagnetic simulations were obtained with W = 20 [μm], which fulfills the mechanical restriction imposed by the bondigs, and are presented in figure 6.7. It is possible to see that the reflections and the insulation are below -10 [dB] in all the bandwidth, which satisfies the requirements, ensuring that little power is reflected. It is also possible to observe that the gain imbalance is lower than in the initial design obtained in AWR.

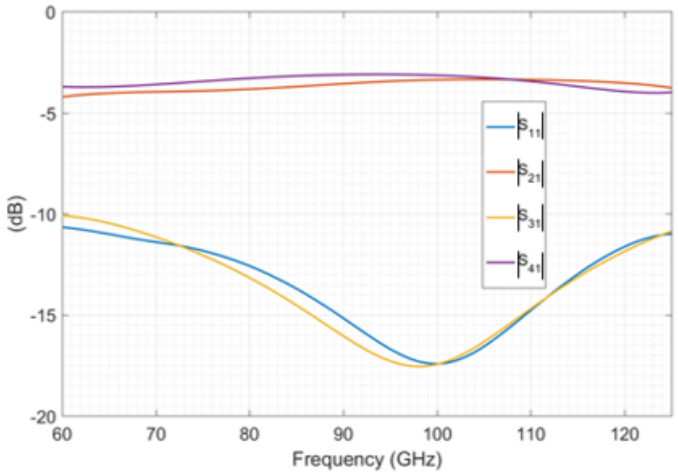

Figure 6.7: S-parameters of the simulated lange coupler in HFSS.

The designing was extremely difficult because changing the parameters to decrease the reflections also affected the gain imbalance and the phase imbalance. In figures 6.8 a and b it is possible to observe the gain imbalance and the phase imbalance obtained with different values for the width of the tracks.

Figure 6.8 a shows that the best gain balance is for W=20 [μm], getting 0.5 [dB]. For a greater width of the tracks of W = 25 [μm], a greater gain imbalance of less than 0.9 [dB] is obtained over the entire bandwidth.

Figure 6.8 b shows that the phase imbalance for the design without mechanical constraints W=10 [μm] is less than 4° over the entire frequency range. When instead, the width of the tracks increases it generates an increase of the phase imbalance, in the case of W = 25 [μm] the gain imbalances is lower than 9°.

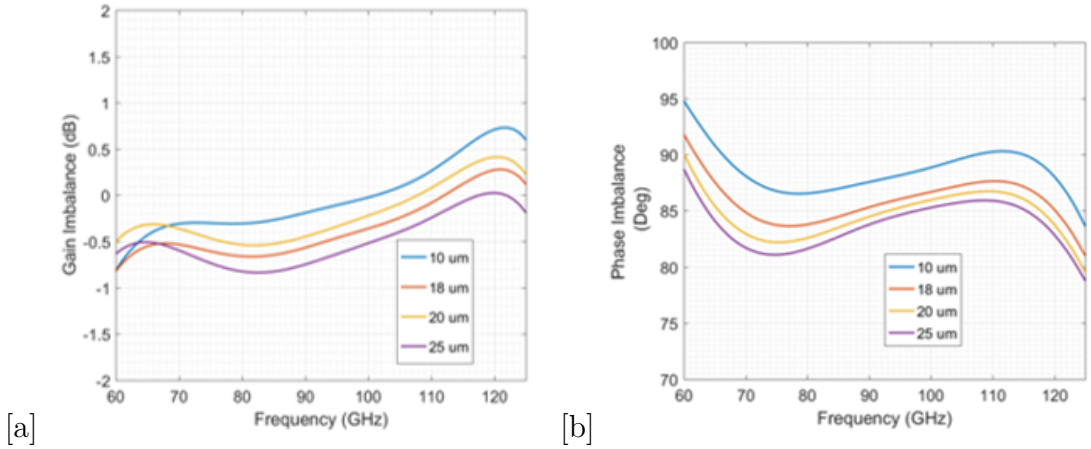

[a] [b]

Figure 6.8: a) Gain imbalance without and with mechanical constraints simulated in HFSS. b) Phase imbalance without and with mechanical constraints simulated in HFSS.

With the results obtained from gain imbalance and phase imbalance we proceeded to plot the sideband rejection of the lange coupler as a function of frequency with the equation 6.3, as seen in the figure 6.9.

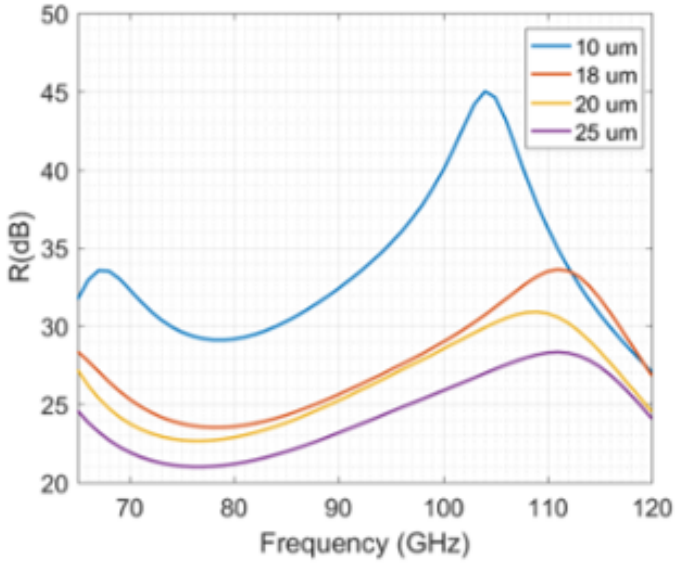

Figure 6.9: Response of the Sideband Rejection on the frequency.

The rejection of the image band would be total if the structure were perfectly balanced, which means that the gain imbalance and phase imbalance would be both 0, a situation that does not occur in practice. Instead, the situation in figure 6.9 is the actual case. In this analysis, it is observed that the sideband rejection is not flat but is rather affected mainly by the high phase imbalance at low frequencies. In the design with the mechanical restrictions, the sideband rejection obtained is higher than 29 [dB] across the bandwidth. On the other hand, as we increase the width of the tracks, the rejection of the lateral band decreases considerably until the extreme case of W = 25 [μm] where this is greater than 21 [dB] in the whole bandwidth.

6.3 Conclusion

In this chapter a lange coupler for the W band was designed based on microstrip technology. From the results obtained through the simulations in HFSS, it was possible to observe that the reflections and the insulation are below -10 [dB] in all the bandwidth. It can also be concluded that the gain imbalance is less than 0.5 [dB] in all the bandwidth for the design made with W=20 [μm], and that the imbalance phase is less than 8^o in the whole bandwidth. With this results, it is possible to obtain a sideband rejection greater than 22 [dB] over the entire bandwidth, which satisfies the requirements.

From the simulations, it was also possible to observe that the results could be improved if the size of the tracks were reduced from 18 to 10 [μm]. This could be possible if the manufacturing of the circuit with the included bondings were done in some MMIC company.

It could also be important to explore the design with another dielectric such as Gallium Arsenide.

In order to further improve the performance, a digital IF hybrid will be implemented. This will correct the phase imbalance results and it has already been tested in the millimeter wave laboratory of the University of Chile, which allows the increase of the sideband rejection.

Chapter 7

CONCLUSIONS

In this thesis, the design, construction, and characterization of key components for a 2SB compact module were presented. The components are a power Amplifier, an Equalizer, an edge coupled microstrip passband Filter, and a Lange coupler.

First, we designed and built a power amplifier based on the integrated circuit HCM1144 that operates in the WR19 band (39.2-59.6 [GHz]). This MMIC presents the inputs and outputs internally matched to 50 [Ω], for which a waveguide transition to microstrip based on a radial antenna was designed. This transition was manufactured with a higher precision and later characterized by the Spectrum Analyzer PXA. Subsequently, the block that contains the amplifier, the transmission lines of 50 [Ω], and the polarization circuits were manufactured. Once the different components for the operation of the amplifier were built, they were assembled and the electrical connections were made with a bonding machine.

The results obtained from the characterization of the amplifier do not agree with the values delivered by the manufacturer, and a lower gain than expected was obtained. The low performance can be attributed to the losses associated with the transition and the length of the bondings.

The performance of the equipment in saturation was also characterized, obtained in one of the configurations an output power greater than 12 [dBm] which is greater than the 6 [dBm] required for the operation of the mixer, fulfilling the requirements.

To get better performance a new block was designed, it unified the 3 blocks in only one, reducing the size of the block and of the length of the bondings. This new design is currently being manufactured.

Was designed, a microwave gain equalizer for the W band, based on 2 resonator branches with an integrated thin film resistor. This equalizer will compensate for the gain imbalance obtained in the first stage of amplification, which is fundamental for any receiver.

The equalization obtained in the simulations carried out in HFSS was approximately 4.3 [dB] in the entire W band. A maximum equalization of approximately 8 [dB] between 73 to 110 [GHz]. Although an equalization of 5 [dB] is desired across the bandwidth, this was

not possible to achieve due to mechanical restrictions imposed in the design. Currently, we are working on the manufacture of the equalizer in the laser LPKF printer of the Millimeter Wave Laboratory. The corresponding block also is being manufactured, which will allow the assembling of the equalizer.

Another fundamental component to the receiver operation is the filter. It was designed based on coupled transmission lines. A first design was made based on the mechanical restriction imposed by the technology available in the DAS. However, this did not comply with the minimum requirements, since it did not cover the entire bandwidth desired 67 to 116 [GHz] and presented high reflections. For this reason, a new filter was designed based on the Iom Beam Milling technology, reducing the losses by return to -12 [dB] in almost the entire bandwidth, except under 72 [GHz] where they are less than -9[dB], and also gave insertion losses less than -0.5 [dB] between 75 to 105 [GHz], and outside of this range decreases a little more.

Finally, the last component to be designed was a lange coupler based on microstrip technology for the W band. Two designs were made: the first was based on the Iom Beam Milling technology with the width and space between lines greater than or equal to 10 [μm]. In the others designs a mechanical restriction of width lines larger than or equal to 18 [μm] was imposed, because it is necessary to make the electrical connections using bondings. The experimental results for the designs with mechanical restriction show that the sideband rejection greater than 20 [dB] over the entire bandwidth, which satisfies the requirements. Furthermore, it was possible to observe that the results could be improved by eliminating mechanical design restrictions such as minimum track width from 18 to 10 [μm] when manufacturing the circuit with the bondings included in some MMIC company.

Bibliography

[1] Thompson, Anthony Richard, James M. Moran, and George Warner Swenson. *Interferometry and synthesis in radio astronomy* , Berlin: Springer, 2017.

[2] Stéphane Paltani. *The Cosmic Microwave Background*, Département d'astronomie, Université de Genève Cosmologie I.

[3] A B Peck, A J Beasley. *High resolution sub-millimeter imaging with ALMA*, (2017).

[4] Otárola, A., et al. *ALMA Memo 512 Atmospheric Transparency at Chajnantor*, 1973-2003. (2005).

[5] Millimeter Atacama Large. *submillimeter Array*, ALMA Santiago Central Offices, Alonso de Cordova 3107, 763-0355, (2014).

[6] ALMA (ESO / NAOJ / NRAO). *ALMA Newsletter N5*, 2010.

[7] ESO/JAO. *https://www.eso.org/public/chile/images/cryostat-1-cc/*, 2016.

[8] DAS. *http://www.das.uchile.cl*.

[9] Sieth, Matthew, et al. *Technology developments for a scalable heterodyne MMIC array at W-band.*, Microwave Conference (EuMC), 2011 41st European. IEEE, 2011.

[10] Yu, Kyung-Wan, et al. *Low noise K-band MMIC receiver module*, IEICE Transactions on Electronics 83.5, 750-754, (2000).

[11] Puetz, P., et al. *345 GHz prototype SIS mixer with integrated MMIC LNA* , International journal of infrared and millimeter waves 27.10, 1365-1379, (2006).

[12] Chattopadhyay, Goutam, et al. *Terahertz array receivers with integrated antennas* , Antenna Technology (iWAT), 2012 IEEE International Workshop on. IEEE, 2012.

[13] Jackson, Bradley. *Subharmonic mixers in CMOS microwave integrated circuits* , Diss. 2009.

[14] González Mariscal, Elena. *Diseño de un mezclador subarmónico en banda W para aplicaciones de Radiometría* , (2015).

[15] Pearman, Dominic. *Electrical characterisation and modelling of Schottky barrier metal source/drain MOSFETs. Diss* , University of Warwick, 2007.

[16] Jesús del Alamo. *course materials for 6.720J Integrated Microelectronic Devices* , Spring 2007.

[17] Echalecu Biurrun, Rubén. *Desarrollo de un receptor sub-armónico de doble conversión a 440GHz.*, (2014).

[18] Olivos Rafael Ignacio Rodríguez, et al. *Design, Construction and Testing of a 2SB Receiver for the Southern Millimeter-Wave Telecope.*

[19] Victor Belitsky *Technologies for mm and sub-mm waves sideband separating receivers*, Group for Advanced Receiver Development (GARD) Earth and Space Science Department Chalmers University of Technology Gothenburg.

[20] Kooi JW. *Advanced receivers for submillimeter and far infrared astronomy* , Rijkuniversit, 2008 Dec.

[21] Lamb, James W., et al. *Sideband-separating MMIC receivers for observation in the 3-mm band* , Millimeter, Submillimeter, and Far-Infrared Detectors and Instrumentation for Astronomy VIII. Vol. 9914. International Society for Optics and Photonics, 2016.

[22] Henderson, Bert C., and James A. Cook. *Image-reject and single-sideband mixers* , Wi TechNote 12.3 (1985).

[23] Armin Walter Doerry. *Noise and Noise Figure for Radar Receivers* , Technical Report, 2016.

[24] OMMIC. *CGY2190UH/C2 Datashett* .

[25] Claudio Jarufe.*DEVELOPMENT OF MODULAR COMPONENTS FOR RADIO ASTRONOMICAL RECEIVERS IN THE BANDS Q (30 50 GHZ) AND W (80 110 GHZ)*, Universidad de Chile, 2018.

[26] By Frederick H. Raab, Peter Asbeck, Steve Cripps, Peter B. Kenington, Zoya B. Popovic, Nick Pothecary, John F. Sevic and Nathan O. Sokal. *RF and Microwave Power Amplifier and Transmitter Technologies*, High Frequency Electronics, (2003).

[27] Dr Veeraiyah Thangasamy, Muhammad Faiz Bukhori, N.A. Kamsani, and Mohd Nizar Hamidon. *An Overview of RF Power Amplifier Techniques and Effect of Transistor Scaling on Its Design Parameters*,International Journal of Applied Engineering Research 9(2):257-276, January 2014.

[28] Del Alamo, Jesus A. *The high-electron mobility transistor at 30: impressive accomplishments and exciting prospects* , (2011).

[29] ANALOG DEVICES. *HMC1144 datasheet* .

[30] Pozar, David M. *Microwave Engineering 3e* .

[31] F. Caspers CERN. *RF engineering basic concepts: S-parameters* , Geneva, Switzerland.

[32] Mata Roca, Salvador. *Transición guía de onda-línea microstrip en banda W* , Universidad de Chile, (2011).

[33] Jarufe Troncoso, Claudio Felipe. *Diseño y Fabricación de un Amplificador de Microondas de Bajo Ruido para la Banda de 31–45 GHz.*, (2010).

[34] Leong, Yoke-Choy, and Sander Weinreb. *Full band waveguide-to-microstrip probe transitions* , Microwave Symposium Digest, 1999 IEEE MTT-S International. Vol. 4. IEEE, 1999.

[35] Van Heuven, J. H. C. *A New Integrated Waveguide-Microstrip Transition (Short Papers*, IEEE Transactions on Microwave Theory and Techniques 24.3, 144-147, (1976).

[36] Kooi, J. W., et al..*A* full-height waveguide to thin-film microstrip transition with exceptional RF bandwidth and coupling efficiency., International Journal of Infrared and Millimeter Waves 24.3, 261-284, (2003).

[37] Sungtek Kahng. *Developing the 150%- FBW Ku-Band Linear Equalizer* , 2010.

[38] Fejzuli, Alen, Ray Kaarsberg, and Nelson Roldan. *Broadband amplifier gain slope equalization with a single passive component* , High Frequency Electronics 5.6, 22-26, (2006).

[39] Zhao, Daqian, Yating Huang, and Li Wang *The design of microstrip gain equalizer in 2–6GHz.*, Computational Problem-solving (ICCP), 2013 International Conference on. IEEE, 2013.

[40] Wang, Huan, et al. *A broadband microwave gain equalizer* , Progress In Electromagnetics Research 33, 63-72, (2012).

[41] Zhou, Peihan, et al. *A new research of broadband microwave gain equalizer.*, Microwave and Millimeter Wave Circuits and System Technology (MMWCST), 2012 International Workshop on. IEEE, 2012.

[42] Qian Ma and Mingbo Ma. *Broadband Amplier Gain Slope Equalization Filter* , University, China.

[43] HFSS. *Lumped RLC Elements in HFSS version 8*, Ansoft HFSS Engineering Note.

[44] Shakdwipee, Pawan, and Kirti Vyas. *Design Edge-Coupled Stripline Band Pass Filter at 39 GHz*, International Journal of Emerging Technology and Advanced Engineering (2013).

[45] Alaydrus, Mudrik. *Designing microstrip bandpass filter at 3.2 GHz* , International Journal on Electrical Engineering and Informatics 2.2, 71-83, (2010).

[46] Inder Pal Singh, Praveen Bhatt, Ajay S. Yadav. *Merits of Parallel Coupled Bandpass*

Filter over end Coupled Bandaoo Filter in X Band, International Journal of Electrical, Electronics and Data Communication, ISSN: 2320-2084, May-2015.

[47] Md Rasheduzzaman Al-Amin, Md. Omar Faruk Chowdhury. *Design and Simulation of Fifth Order Band-Pass Filter for S Band* , Dept. of EEE, Bangladesh University of Business and Technology, Mirpur, Dhaka, Bangladesh, March 2016.

[48] Sharma, Girraj, et al. *Half-wavelength parallel edge coupled filter simulation using Matlab* , International Journal of Innovative Research in Computer and Communication Engineering 1.2, 248-253, (2013).

[49] Wai, Hnin Yu, et al. *Design and simulation of edge-coupled stripline band pass filter for Ka band application* , International Conference on Trends in Electrical, Electronics and Power Engineering (ICTEEP'2012) July. 2012

[50] Simons, Rainee N. *Coplanar waveguide discontinuities and circuit elements* , Coplanar Waveguide Circuits, Components, and Systems, 237-287, (2001).

[51] Rani, Pooja, Shilpi Gupta, and R. K. Prasad. *"Design optimization of microstrip parallel coupled bandpass Filter at 20 GHz."* International Journal of Advanced Research in Computer Engineering Technology (INJARCET) (2014).

[52] Srinath, S. *Design of 4th Order Parallel Coupled Microstrip Bandpass Filter at Dual Frequencies of 1.8 GHz and 2.4 GHz for Wireless Application* , International Journal of Innovative Research in Computer and Communication Engineering 2.6, 4744-51, (2014).

[53] Design and Simulation of Edge-coupled Stripline Band Pass Filter for Ka Band Application Hnin Yu Wai, Zaw Min Naing, Kyaw Soe Lwin and Hla Myo Tun

[54] Satya Sai Srikant. *An overview on Monolithic Microwave Integrated Circuits*, Department of Electronics and Communication Engineering SRM University, Modinagar, Ghaziabad, January 2014.

[55] J. Lange. *Tnterdigitated stnpline quadrature hybnd*, IEEE Trans. Micmvaoe Theory Tech., vol. M'IT-17, pp. 1150-1151, Dec. 1969.

[56] Kajfez, Darko, Zoja Paunovic, and Stane Pavlin. *Simplified design of Lange coupler* , IEEE Transactions on Microwave Theory and Techniques 26.10, 806-808, (1978).

[57] Agilent EEsot EDA. *Overview on Lange Coupler Design.*

[58] Azar, Mohammad Nikfal, Manochehr Kamyab, and Mehrdad Djavid. *Design and Manufacturing the Balance Amplifier Using the Lange Coupler in X-Band* , Session 3AP: 205.

[59] Grebennikov, Andrei. "Power combiners, impedance transformers and directional couplers." High Freq. Electron 6.12 (2007): 20-38.

[60] Galíp Orkun Arican. *Electromagnetic Analysis and design of Miniaturized Branchline Couplers*, A Thesis submitted to the Graduate School of Natural and Applied Science of

Middle East Technical University.

[61] Tutkur, Elmin. *Wideband Directional Couplers and Power Splitters* , Unpublished Master of Science Thesis, Chalmers University of Technology (2014).

[62] Lamb, James W., et al. *Sideband-separating MMIC receivers for observation in the 3-mm band* , Millimeter, Submillimeter, and Far-Infrared Detectors and Instrumentation for Astronomy VIII. Vol. 9914. International Society for Optics and Photonics, 2016.

[63] Claude, S. M. X., et al. *Design of a sideband-separating balanced SIS mixer based on waveguide hybrids*, ALMA Memo 316 (2000).

[64] Sobis, Peter J., Anders Emrich, and Jan Stake. *A low VSWR 2SB schottky receiver*, IEEE Transactions on Terahertz Science and Technology 1.2, 403-411, (2011).

[65] Alvear, Andrés, et al. *"FPGA-based digital signal processing for the next generation radio astronomy instruments: ultra-pure sideband separation and polarization detection."* Millimeter, Submillimeter, and Far-Infrared Detectors and Instrumentation for Astronomy VIII. Vol. 9914. International Society for Optics and Photonics, 2016.